Chirality-induced signals in coherent multidimensional spectroscopy of excitons

Darius Abramavicius
Theoretical Physics Department, Faculty of Physics of Vilnius University, Sauletekio Avenue 9, Building 3, 10222 Vilnius, Lithuania

Shaul Mukamel[a)]
Chemistry Department, University of California, Irvine, California 92697-2025

(Received 1 August 2005; accepted 12 September 2005; published online 20 January 2006)

The nonlocal second- and third-order susceptibilities of an isotropic ensemble of aggregates are calculated by solving the nonlinear exciton equations which map the system into coupled anharmonic oscillators. Both electric and magnetic contributions are included using the minimal-coupling Hamiltonian. The various tensor components are evaluated to first order in the optical wave vector **k**. Additional structural information about the interchromophore distances, which is not accessible through zeroth-order contributions (the dipole approximation), is contained to the first order in **k**. New resonant second- and third-order signals predicted for chiral molecules provide multidimensional extensions of circular dichroism spectroscopy. Numerical simulations demonstrate the sensitivity of third-order signals to the secondary structural motiffs of peptides. © *2006 American Institute of Physics*. [DOI: 10.1063/1.2104527]

I. INTRODUCTION

Circular dichroism (CD) is a widely-used linear spectroscopic tool for molecular structure determination.[1] This signal is finite to the first order in the optical wave vector **k**, but vanishes within the dipole approximation where we set **k** =0. The CD spectrum changes its sign for optically active molecules with an opposite sense of chirality [levo (L) or its mirror image dextro (D), which cannot be superimposed with each other by translation and rotation operations]. Optical response functions must be either even or odd with respect to the parity operation. The former, labeled as nonchiral (NC), are insensitive to chirality whereas the latter are chirality induced (CI) since they vanish for nonchiral molecules and for racemates. The chiral properties of molecules have been extensively probed using CD and Raman optical activity (ROA), which are the simplest examples of CI signals.[2–6] Due to its high sensitivity, the CD spectroscopy of electronic transitions (ECD) in the visible and the UV has become an important tool for the structure determination of proteins.[1,7–10] Since it discriminates between protein secondary structural motiffs such as helices and sheets[11–13] the technique provides an effective tool for probing folding dynamics.

Nonlinear optical techniques have the capacity to probe doubly excited (two-exciton) molecular states as well as certain dipole elements which are not accessible through CD and ROA.[14–17] Buckingham and Fischer have shown that parity-odd time-even molecular property tensors have nonvanishing isotropic components, giving rise to finite signals in noncentrosymmetric liquids of chiral molecules.[18] Examples of which are $\chi^{(1)}$ calculated to first order in the optical wave vector **k** (CD) and $\chi^{(2)}$ to zero order. $\chi^{(2)}$ could provide more valuable information compared with CD regarding the electronic structure and stereochemistry of molecules. Observing it in liquids requires special experimental conditions: To the zero order in **k**, sum and difference frequency generations can only be observed in non-phase-matching directions.[19,20] This has been realized experimentally using a noncollinear laser configuration[20] and predicted in highly focused Gaussian laser fields where a Gaussian packet of wave vectors and of optical polarizations generates the signal in a collinear laser configuration.[21] Second-order in vibrational spectroscopy was recently discussed with applications to sum frequency generation with circularly polarized beams[22,23] and the Raman-induced Kerr optical activity.[24]

In this paper we calculate the linear, second- and third-order susceptibilities of molecules made of coupled chromophores to first order in the wave vector and predict new nonlinear families of CI tensor components which can be detected by specific configurations of optical-field polarizations.

The Frenkel exciton Hamiltonian is introduced in Sec. II. This model has been widely used for calculating electronic and vibrational excitations in molecular aggregates (J aggregates,[25] and biological light harvesting (LH) systems[26]), conjugated polymers, and molecular crystals[27] as well as polypeptides.[14,28–33] In the Heitler-London approximation its energy spectrum consists of decoupled manifolds: the ground state, one exciton, two exciton, etc.[34] The role of the various manifolds in specific resonant optical techniques can be clearly separated by invoking the rotating-wave approximation (RWA). We use the minimal-coupling Hamiltonian (Appendix A) to describe the interaction with the electromagnetic field. Electric and magnetic moments then enter more naturally than in the multipolar Hamiltonian. The

[a)]Electronic mail: smukamel@uci.edu

nonlinear response functions are defined in Sec. III. The symmetries of the nonlinear signals to the first order in the wave vector and their relation to chirality are surveyed in Sec. IV. The required orientational averagings of transition currents are given in Appendix B. The nonlinear exciton equations (NEEs) are derived in Appendix C and the lowest three susceptibilities and response functions calculated using their Green's-function solutions are given in Sec. V. Two-exciton resonances, which are important for second- and third-order spectroscopies, are obtained from the exciton scattering matrix;[35–38] it is not necessary to compute the two-exciton eigenstates, which is very expensive numerically. For localized excitons and short-range anharmonicities, calculating the exciton scattering matrix involves the same effort as the one-exciton eigenvalue problem. The linear-response functions are derived in Appendix D. The NEE for second-order signals are given in Appendix E and the response functions for sum frequency generation (SFG) and difference frequency generation (DFG) are calculated in Appendix F. The previously derived expressions for the third-order signals[36,37] are generalized to include magnetic properties through transition currents. The numerical calculations for vibrational excitons in the parallel and antiparallel β-sheet structural motiffs of peptides are presented and discussed in Sec. VI.

II. THE MINIMAL-COUPLING EXCITON HAMILTONIAN

We consider a system of $\mathcal{N}$-coupled vibrational or electronic chromophores (oscillators) described by the following Frenkel exciton Hamiltonian:

$$\hat{H} = \sum_m \varepsilon_m \hat{B}_m^\dagger \hat{B}_m + \sum_{mn}^{m\neq n} h_{m,n} \hat{B}_m^\dagger \hat{B}_n + \sum_{mn,m'n'} U_{mn,m'n'} \hat{B}_m^\dagger \hat{B}_n^\dagger \hat{B}_{m'} \hat{B}_{n'} + \hat{H}'. \quad (1)$$

The creation and annihilation operators for chromophore m, $\hat{B}_m^\dagger$, and $\hat{B}_m$, satisfy the boson, $[\hat{B}_m, \hat{B}_n^\dagger] = \delta_{mn}$, commutation relations. The first two terms constitute a harmonic free-boson Hamiltonian: ε_m is the frequency of mode m, and the quadratic intermode coupling h_{mn} is calculated in the Heitler-London approximation where off-resonant $\hat{B}_m^\dagger \hat{B}_n^\dagger$ and $\hat{B}_m \hat{B}_n$ terms are neglected. U represents a quartic anharmonicity. The boson representation is most suitable for vibrational excitons. Electronic excitations are commonly described using two-level chromophores by setting $U_{nnnn} \to +\infty$.[39]

Only the one-exciton manifold is relevant for linear spectroscopies. These states are obtained by diagonalizing the following relatively small one-exciton block of the Hamiltonian:

$$\sum_n h_{m,n} \psi_{\xi n} = E_\xi \psi_{\xi m}, \quad (2)$$

giving the one-exciton energies E_ξ and eigenfunctions $\psi_{\xi m}$.

We shall describe the interaction with the optical field using the following minimal-coupling (p.A) Hamiltonian (see Appendix A):[40,41]

$$\hat{H}'(t) = -\frac{1}{c} \int d\mathbf{r} [\hat{\mathbb{J}}(\mathbf{r}) \cdot \mathbb{A}(\mathbf{r},t) + \hat{Q}(\mathbf{r}) \mathbb{A}^2(\mathbf{r},t)], \quad (3)$$

where $\mathbb{A}(\mathbf{r},t)$ is the transverse vector potential $[\mathbb{A}^2(\mathbf{r}_m,t) \equiv \mathbb{A}(\mathbf{r}_m,t) \cdot \mathbb{A}(\mathbf{r}_m,t)]$. $\hat{\mathbb{J}}$ and $\hat{Q}$ are the current and the charge-density operators, respectively. Expanding them in exciton operators (see Appendix A) we get

$$\hat{\mathbb{J}}(\mathbf{r}) = \sum_m \delta(\mathbf{r}-\mathbf{r}_m)[\boldsymbol{j}_m^* \hat{B}_m^\dagger + \boldsymbol{j}_m \hat{B}_m + \boldsymbol{f}_m \hat{B}_m^\dagger \hat{B}_m + \boldsymbol{g}_m^* \hat{B}_m^{\dagger 2} + \boldsymbol{g}_m \hat{B}_m^2], \quad (4)$$

$$\hat{Q}(\mathbf{r}) = \sum_m \delta(\mathbf{r}-\mathbf{r}_m)[j_m'^* \hat{B}_m^\dagger + j_m' \hat{B}_m + f_m' \hat{B}_m^\dagger \hat{B}_m + g_m'^* \hat{B}_m^{\dagger 2} + g_m' \hat{B}_m^2], \quad (5)$$

where the sum is over all chromophores. $\boldsymbol{j}_m$ is the transition current density, a complex vector with the components $(\boldsymbol{j}_m^x, \boldsymbol{j}_m^y, \boldsymbol{j}_m^z)$, of chromophore m, located at $\mathbf{r}_m$, and $\boldsymbol{f}_m$ is its permanent current in the excited state, while $\boldsymbol{g}_m$ is a quadratic transition current which can create double-quantum coherences (overtones). j_m', f_m', and g_m' are defined similarly.

When the electromagnetic field is switched off, our Hamiltonian becomes block diagonal in the number of excitons given the ground state $|0\rangle$, the one-exciton block $\hat{B}_m^\dagger|0\rangle$, the two-exciton block $\hat{B}_n^\dagger \hat{B}_m^\dagger|0\rangle$, etc. With the coupling [Eqs. (3)–(5)] only one- and two-exciton states are required for the spectroscopies to third and lower orders.

The induced current $\mathbb{J}$ has electric (such as induced dipoles) as well as magnetic (angular momentum) contributions and serves as a source in the following Maxwell equations for the signal electric field:

$$\nabla \times \nabla \times \mathbb{E} + \frac{1}{c^2} \frac{\partial^2}{\partial t^2} \mathbb{E} = -\frac{4\pi}{c^2} \frac{\partial \mathbb{J}}{\partial t}. \quad (6)$$

Predicting the linear and nonlinear properties of molecules depends on the calculation of $\mathbb{J}$, which will be the focus of the remainder of this article.

III. RESPONSE FUNCTIONS FOR RESONANT *n*-WAVE MIXING

The nonlinear optical experiment is depicted in Fig. 1. The incoming laser fields interact with the sample. The induced nonlinear polarization and magnetization then act as a source of the signal field. To describe both the electric and the magnetic responses we define the nth-order response function $R^{(n)}$ which connects the incoming vector potential to the following induced nonlinear current:[42]

$$\mathbb{J}_{\nu_S}^{(n)}(\mathbf{r}_S \tau_S) = \sum_{\nu_n \cdots \nu_1} \int d\mathbf{r}_n \cdots \int d\mathbf{r}_1 \int d\tau_n \cdots \int d\tau_1 R_{\nu_S,\nu_n \cdots \nu_1}^{(n)}(\mathbf{r}_S \tau_S, \mathbf{r}_n \tau_n, \ldots, \mathbf{r}_1, \tau_1) \times \mathbb{A}_{\nu_n}(\mathbf{r}_n, \tau_n) \cdots \mathbb{A}_{\nu_1}(\mathbf{r}_1, \tau_1). \quad (7)$$

τ_j and $\mathbf{r}_j$ denote the times and coordinates of the various interactions with the fields. The Fourier transformation of $\mathbb{J}$

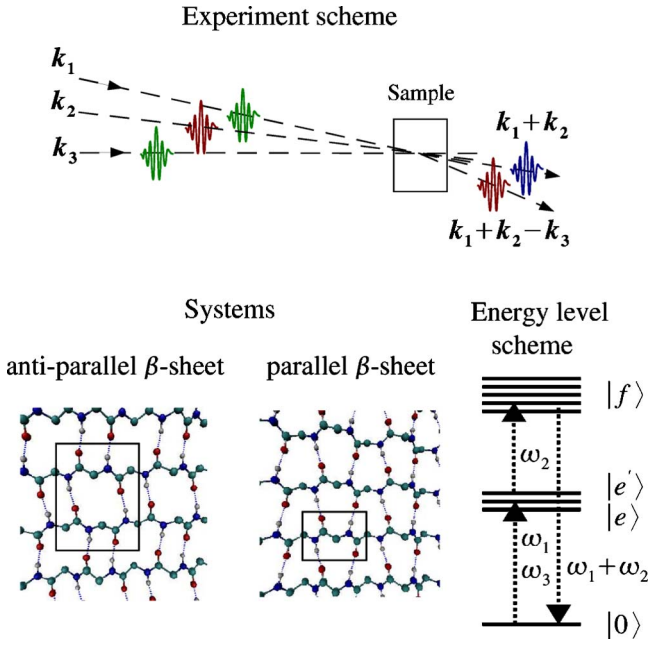

FIG. 1. Upper panel: Experimental setup for nonlinear optical signals. Lower panel: The secondary peptide structures studied.

and $\mathbb{A}$ to the momentum-frequency $(\mathbf{k}\omega)$ domain $F(\mathbf{k}\omega)=\int dt\int d\mathbf{r}F(\mathbf{r}t)e^{-i\mathbf{k}r+i\omega t}$ (Ref. 43), gives

$$\mathbb{J}^{(n)}_{\nu_S}(\mathbf{k}_S\omega_S)=\frac{1}{(2\pi)^{4n}}\sum_{\nu_n\cdots\nu_1}\int d\mathbf{k}_n\cdots\int d\mathbf{k}_1\int d\omega_n\cdots\int d\omega_1 X^{(n)}_{\nu_S\nu_n\cdots\nu_1}(-\mathbf{k}_S-\omega_S,\mathbf{k}_n\omega_n,\ldots,\mathbf{k}_1\omega_1)\times\mathbb{A}_{\nu_n}(\mathbf{k}_n,\omega_n)\cdots\mathbb{A}_{\nu_1}(\mathbf{k}_1,\omega_1). \quad (8)$$

The nth-order susceptibility $X^{(n)}$ is connected to $R^{(n)}$ by a Fourier transform,

$$X^{(n)}_{\nu_S\cdots\nu_1}(-\mathbf{k}_S-\omega_S,\mathbf{k}_n,\omega_n,\ldots,\mathbf{k}_1,\omega_1)=\int d\tau_S\int d\mathbf{r}_S\int d\tau_n\int d\mathbf{r}_n\cdots\int d\tau_1\int d\mathbf{r}_1 R^{(n)}_{\nu_S\nu_n\cdots\nu_1}(\mathbf{r}_S\tau_S,\mathbf{r}_n\tau_n,\ldots,\mathbf{r}_1\tau_1)\times e^{i\omega_s\tau_s-i\mathbf{k}_s\mathbf{r}_s-i\omega_n\tau_n+i\mathbf{k}_n\mathbf{r}_n\cdots-i\omega_1\tau_1+i\mathbf{k}_1\mathbf{r}_1}. \quad (9)$$

$R^{(n)}$ can be defined to be symmetric with respect to the permutation of the optical-field indices: $\nu_l\mathbf{r}_l\tau_l$ with $l=1,\ldots,n$. Similarly, the susceptibility is symmetric with respect to the permutations of $\nu_l\mathbf{k}_l\omega_l$.

In this paper we will calculate $X^{(n)}$ and $R^{(n)}$. Optical signals are commonly calculated using a different susceptibility $\chi^{(n)}$, which connects nonlinear polarization $\mathbb{P}^{(n)}_{\nu_S}$ with the incoming electric fields $\mathbb{E}$ (rather than $\mathbb{J}$ and $\mathbb{A}$):

$$\mathbb{P}^{(n)}_{\nu_S}(\mathbf{k}_S\omega_S)=\frac{1}{(2\pi)^{4n}}\sum_{\nu_n\cdots\nu_1}\int d\mathbf{k}_n\cdots\int d\mathbf{k}_1\int d\omega_n\cdots\int d\omega_1 \chi^{(n)}_{\nu_S\nu_n\cdots\nu_1}(-\mathbf{k}_S-\omega_S,\mathbf{k}_n\omega_n,\ldots,\mathbf{k}_1\omega_1)\times\mathbb{E}_{\nu_n}(\mathbf{k}_n,\omega_n)\cdots\mathbb{E}_{\nu_1}(\mathbf{k}_1,\omega_1). \quad (10)$$

Noting that for transverse fields $\mathbb{E}(\mathbf{r}t)=-(1/c)(\partial/\partial t)\mathbb{A}(\mathbf{r}t)$ (and the scalar potential can be neglected), we get $\mathbb{E}(\mathbf{k}\omega)=(i/c)\omega\mathbb{A}(\mathbf{k}\omega)$. From the charge continuity relation we have $\mathbb{J}(\mathbf{r}t)=(\partial/\partial t)\mathbb{P}(\mathbf{r}t)$ which in the Fourier space gives $\mathbb{J}(\mathbf{k}\omega)=-i\omega\mathbb{P}(\mathbf{k}\omega)$. $\mathbb{P}$ includes also the magnetic properties of the material through the current. $\chi^{(n)}$ is, thus, simply related to $X^{(n)}$,

$$X^{(n)}_{\nu_S\cdots\nu_1}(-\mathbf{k}_S-\omega_S,\mathbf{k}_n,\omega_n,\ldots,\mathbf{k}_1,\omega_1)=\frac{i^{n-1}}{c^n}\omega_S\omega_n\cdots\omega_1\chi^{(n)}_{\nu_S\nu_n\cdots\nu_1}(-\mathbf{k}_S-\omega_S,\mathbf{k}_n\omega_n,\ldots,\mathbf{k}_1\omega_1). \quad (11)$$

A similarly simple relation may be obtained in the time domain by assuming the slowly varying amplitude approximation.[44]

A. Frequency-domain techniques

The $(n+1)$-wave-mixing signals are induced by n incoming laser fields with wave vectors $\mathbf{k}_l$ $(l=1,\ldots,n)$ described by the following vector potential:

$$\mathbb{A}(\mathbf{r},\tau)=\frac{1}{2}\sum_l A^{(l)}_0\mathbf{e}_l\exp(i\mathbf{k}_l\mathbf{r}-i\omega_l\tau)+\text{c.c.}, \quad (12)$$

where $A^{(l)}_0$ is the lth field amplitude, $\mathbf{e}_l$ is its unit polarization vector, $\mathbf{k}_l=(\omega_l/c)\mathbf{n}_l$ is the wave vector ($\mathbf{n}_l$ is a unit vector), ω_l is the carrier frequency, c is the speed of light, and c.c. denotes the complex conjugate. For transverse optical fields $\mathbf{e}_l\cdot\mathbf{n}_l=0$. In $\mathbf{k}\omega$ space we have

$$\mathbb{A}(\mathbf{k},\omega)=\frac{(2\pi)^4}{2}\sum_l A^{(l)}_0\mathbf{e}_l[\delta(\mathbf{k}-\mathbf{k}_l)\delta(\omega-\omega_l)+\delta(\mathbf{k}+\mathbf{k}_l)\delta(\omega+\omega_l)]. \quad (13)$$

In linear techniques such as absorption and CD the generated field with frequency ω_S polarized along $\mathbf{e}_S$ and propagating with the wave vector $\mathbf{k}_S=(\omega_S/c)\mathbf{n}_S$ is

$$E^{(1)}_{\mathbf{k}_S}\propto\sum_{\nu_S=x,y,z}\mathbb{J}^{(1)}_{\nu_S}(\mathbf{k}_S,\omega_S)\mathbf{e}^{\nu_S}_S=\frac{A^{(1)}_0}{2}\sum_{\nu_S\nu_1}X^{(1)}_{\nu_S\nu_1}(-\mathbf{k}_S,-\omega_S,\pm\mathbf{k}_1\pm\omega_1)\mathbf{e}^{\nu_S}_S\mathbf{e}^{\nu_1}_1. \quad (14)$$

The signal depends on the orientation of a detector and its spectral and temporal resolutions. The signs of the incoming wave vectors and frequencies indicate which component of the incoming optical field [either $e^{i\mathbf{k}r-i\omega t}$ giving $(+\mathbf{k},+\omega)$ or $e^{-i\mathbf{k}r+i\omega t}$ giving $(-\mathbf{k},-\omega)$) had interacted with the system. The complete susceptibility is obtained by selecting different wave vectors and polarizations of the incoming fields.

TABLE I. Contributions to the zeroth and first orders in the wave vector to the molecular polarizabilities α, β, and γ. ν denotes the tensor components. Only electric dipoles enter in the dipole approximation. Both electric and magnetic transitions contribute to the first order in $\mathbf{k}$.

Polarizability	Zeroth order in $\mathbf{k}$ (the dipole approximation)	Parity	First order in $\mathbf{k}$	Parity
α	$\boldsymbol{\mu}^{\nu_2}\boldsymbol{\mu}^{\nu_1}$	+	$\mathbf{k}^{\nu_2+2}\boldsymbol{m}^{\nu_2+1}\boldsymbol{\mu}^{\nu_1}, \mathbf{k}^{\kappa}\mathbf{r}^{\kappa}\boldsymbol{\mu}^{\nu_2}\boldsymbol{\mu}^{\nu_1}$	−
β	$\boldsymbol{\mu}^{\nu_3}\boldsymbol{\mu}^{\nu_2}\boldsymbol{\mu}^{\nu_1}$	−	$\mathbf{k}^{\nu_3+2}\boldsymbol{m}^{\nu_3+1}\boldsymbol{\mu}^{\nu_2}\boldsymbol{\mu}^{\nu_1}, \mathbf{k}^{\kappa}\mathbf{r}^{\kappa}\boldsymbol{\mu}^{\nu_3}\boldsymbol{\mu}^{\nu_2}\boldsymbol{\mu}^{\nu_1}$	+
γ	$\boldsymbol{\mu}^{\nu_4}\boldsymbol{\mu}^{\nu_3}\boldsymbol{\mu}^{\nu_2}\boldsymbol{\mu}^{\nu_1}$	+	$\mathbf{k}^{\nu_4+2}\boldsymbol{m}^{\nu_4+1}\boldsymbol{\mu}^{\nu_3}\boldsymbol{\mu}^{\nu_2}\boldsymbol{\mu}^{\nu_1}, \mathbf{k}^{\kappa}\mathbf{r}^{\kappa}\boldsymbol{\mu}^{\nu_4}\boldsymbol{\mu}^{\nu_3}\boldsymbol{\mu}^{\nu_2}\boldsymbol{\mu}^{\nu_1}$	−

The generated field in an $(n+1)$-wave-mixing experiment is proportional to the optical susceptibility $X^{(n)}_{\nu_S\nu_n\cdots\nu_1}(-\mathbf{k}_S,-\omega_S,\pm\mathbf{k}_n,\pm\omega_n,\ldots,\pm\mathbf{k}_1,\pm\omega_1)$ corresponding to the incoming field configuration $\pm\mathbf{k}_n\pm\cdots\pm\mathbf{k}_2\pm\mathbf{k}_1$,

$$\mathbb{E}^{(n)}_{\mathbf{k}_S} \propto \frac{1}{2^n}A^{(n)}_0\cdots A^{(1)}_0 \sum_{\nu_{n+1}\cdots\nu_1} X^{(n)}_{\nu_{n+1}\cdots\nu_1}(-\mathbf{k}_S,-\omega_S,\pm\mathbf{k}_n,\pm\omega_n,\ldots,\pm\mathbf{k}_1,\pm\omega_1) \times \mathbf{e}_S^{\nu_{n+1}}\mathbf{e}_n^{\nu_n}\cdots\mathbf{e}_1^{\nu_1}. \quad (15)$$

We assume that the signal field with wave vector $\mathbf{k}_S=(\omega_S/c)\mathbf{n}_S$ and frequency $\omega_S=\pm\omega_n\cdots\pm\omega_1$ is measured along $\mathbf{n}_S=(\pm\mathbf{n}_n\cdots\pm\mathbf{n}_1)/|\pm\mathbf{n}_n\cdots\pm\mathbf{n}_1|$. Meeting all these conditions simultaneously (phase-matching) will be addressed later for specific signals.

B. Time-domain techniques

The time-domain $(n+1)$-wave-mixing signals are induced by n short laser pulses,

$$\mathbb{A}(\mathbf{r},\tau)=\frac{1}{2}\sum_l A^{(l)}_0(\tau-\bar{\tau}_l)\mathbf{e}_l\exp(i\mathbf{k}_l\mathbf{r}-i\omega_l\tau)+\text{c.c.}, \quad (16)$$

where $A^{(l)}_0(\tau-\bar{\tau}_l)$ is the amplitude of the lth pulse that peaked at $\bar{\tau}_l$.

In the impulsive limit of short and nonoverlapping pulses, the time integrations in Eq. (7) can be eliminated and the signal field is simply proportional to the response functions $R^{(n)}$. Both real and imaginary parts of $R^{(n)}$ can be measured independently by heterodyne detection.[42] Taking into account time translational invariance we will calculate the signal field as a function of the delay times between incoming pulses: $\mathbb{R}^{(n)}_{\nu_S\nu_n\cdots\nu_1}(\mathbf{k}_S,\pm\mathbf{k}_n,\ldots,\pm\mathbf{k}_1,t_n,\ldots,t_1)\equiv R^{(n)}_{\nu_S\nu_n\cdots\nu_1}(\mathbf{k}_S\tau_S,\pm\mathbf{k}_n\bar{\tau}_n,\ldots,\pm\mathbf{k}_1\bar{\tau}_1)$, where $t_n=\tau_S-\bar{\tau}_{n-1}$ and $t_l=\bar{\tau}_l-\bar{\tau}_{l-1}$ for $l=1,\ldots,n-1$ are time delays between pulses and t_n is the delay between the last pulse and the measurement. We assume that pulse $\mathbf{k}_1$ comes first followed by $\mathbf{k}_2$ and so on, thus, $\tau_S>\bar{\tau}_n>\bar{\tau}_{n-1}>\cdots>\bar{\tau}_1$ and all delay times are positive. $\mathbb{R}^{(n)}_{\nu_S\nu_n\ldots\nu_1}$ represents the signal field polarized along $\mathbf{e}_S$ with the wave vector $\mathbf{k}_S=(\omega_S/c)\mathbf{n}_S$.

Specific nonlinear techniques are obtained by selecting the signs of the optical wave vectors and the frequencies. For slowly varying amplitudes we have the same condition for the generated field as in the frequency domain, i.e., $\omega_S=\pm\omega_n\pm\cdots\pm\omega_1$. Time-domain signals may be displayed by performing the following one-sided Fourier transform with respect to several time delays: $F(\Omega)=\int_0^\infty dt e^{i\Omega t}F(t)$ giving $\mathbb{R}^{(n)}_{\nu_S\nu_n\cdots\nu_1}(\mathbf{k}_S,\pm\mathbf{k}_n,\ldots,\pm\mathbf{k}_1,\Omega_n,\ldots,\Omega_1)$.

IV. WAVE VECTOR EXPANSION AND ORIENTATIONAL TENSOR AVERAGINGS

The microscopic inputs for computing the macroscopic optical response are the linear, quadratic, and cubic molecular polarizabilities: α, β, and γ, respectively: $\chi^{(1)}=\langle\alpha\rangle$, $\chi^{(2)}=\langle\beta\rangle$, and $\chi^{(3)}=\langle\gamma\rangle$, where $\langle\cdots\rangle$ denotes ensemble averaging. We first focus on the current $\mathbb{J}$ contribution to the optical response. The charge-density contribution Q will be addressed later in this section. The polarizabilities are in general related to the multipoint equilibrium correlation functions of the current operators, $\alpha\propto\text{Tr}[\mathbb{J}(\tau)\mathbb{J}(0)\rho]$, $\beta\propto\text{Tr}[\mathbb{J}(\tau_3)\mathbb{J}(\tau_2)\mathbb{J}(\tau_1)\rho]$, and $\gamma\propto\text{Tr}[\mathbb{J}(\tau_4)\mathbb{J}(\tau_3)\mathbb{J}(\tau_2)\mathbb{J}(\tau_1)\rho]$, where ρ is the equilibrium density matrix. We shall examine the symmetry properties of such products. In Appendix A we relate the current operator in $\mathbf{k}\omega$ space with the electric and magnetic transition dipoles. To the first order in the wave vector, the relations between the transition current and electric and magnetic transition dipoles are

$$\boldsymbol{j}_l(\mathbf{k})\approx-i\omega\boldsymbol{\mu}_l-\omega(\mathbf{k}\cdot\mathbf{r}_l)\boldsymbol{\mu}_l+i\mathbf{k}\times\boldsymbol{m}_l, \quad (17)$$

$$\boldsymbol{f}_l(\mathbf{k})\approx-i\omega\boldsymbol{\mu}'_l-\omega(\mathbf{k}\cdot\mathbf{r}_l)\boldsymbol{\mu}'_l+i\mathbf{k}\times\boldsymbol{m}'_l, \quad (18)$$

and

$$\boldsymbol{g}_l(\mathbf{k})\approx-i\omega\boldsymbol{\mu}''_l-\omega(\mathbf{k}\cdot\mathbf{r}_l)\boldsymbol{\mu}''_l+i\mathbf{k}\times\boldsymbol{m}''_l. \quad (19)$$

The first term in each expression is the dipole approximation for the entire aggregate. Magnetic properties enter through the other two terms which are the first order in the wave vector.

In order to relate the signal to molecular chirality we need to inspect its dependence on the parity operation $\mathcal{P}$, which inverts the coordinates of all the particles: $x_i\rightarrow-x_i$, $y_i\rightarrow-y_i$, and $z_i\rightarrow-z_i$.[3,18] $\mathcal{P}$ transforms an isotropic ensemble of chiral molecules into an isotropic ensemble with opposite sense of chirality. The transformation of optical signals with parity will, thus, depend on their chirality. Molecular geometry enters through various transition dipoles (Table I). For example, α in the dipole approximation is related to a product of two electric transition dipoles. To the first order in the wave vector, the contributions to α involve either one mag-

netic dipole or a coordinate $\mathbf{r}$ (distance between two chromophores). The contributions to β and γ are tabulated as well.

$\mathcal{P}$ reverses the sign of both the transition dipole, $\mathcal{P}\boldsymbol{\mu}=-\boldsymbol{\mu}$, and the coordinate, $\mathcal{P}\mathbf{r}=-\mathbf{r}$. However, it does not change the sign of the magnetic transition dipole (which represents an angular momentum), $\mathcal{P}\boldsymbol{m}=\boldsymbol{m}$. The application of two parity operations restores the system back into its original state. Therefore, the system properties can be classified as either parity even ($\mathcal{P}F=F$ denoted by "+") or parity odd ($\mathcal{P}F=-F$ denoted by "–"). $\mathcal{P}$ is intimately related to chirality since it transforms chiral molecules to their enantiomers. Based on these, the various contributions to α, β, and γ may be classified as either parity even or odd depending on the number and type of dipole factors: Parity-even (odd) tensors give the same (inverse) sign of the signal field for the assemblies of chiral molecules and are therefore NC (CI)-type.

A complete three-dimensional orientational averaging needs to be performed in isotropic solutions. The $\mathcal{P}$ symmetry is the same for all the tensor components of a given order. However, isotropic orientational averaging which relates the polarizabilities to the macroscopic susceptibilities $\chi^{(1)}=\langle\alpha\rangle$, $\chi^{(2)}=\langle\beta\rangle$, and $\chi^{(3)}=\langle\gamma\rangle$ adds restrictions on the allowed tensor components.[45] We adopt the notation $\langle \boldsymbol{a}_s^{\nu_s}\cdots\boldsymbol{a}_1^{\nu_1}\rangle \equiv \langle(\boldsymbol{a}_s\cdot\mathbf{e}^{\nu_s})\cdots(\boldsymbol{a}_1\cdot\mathbf{e}^{\nu_1})\rangle$, where $\mathbf{e}$ are unit vectors in the laboratory frame and $\boldsymbol{a}$ is a vector in the molecular frame. These products of projections have simple transformations between coordinate systems, and rotational averagings can be easily carried out.[3,45] An sth-rank product has the following transformation between the molecular and the laboratory frames:

$$\langle \boldsymbol{a}_s^{\nu_s}\cdots\boldsymbol{a}_1^{\nu_1}\rangle = \sum_{\alpha_s\cdots\alpha_1} \mathbf{T}^{(s)}_{\nu_s\cdots\nu_1,\alpha_s\cdots\alpha_1}\boldsymbol{a}_s^{\alpha_s}\cdots\boldsymbol{a}_1^{\alpha_1}, \tag{20}$$

where $\mathbf{T}^{(s)}_{\nu_s\cdots\nu_1,\alpha_s\cdots\alpha_1}=\langle l_{\nu_s\alpha_s}\cdots l_{\nu_1\alpha_1}\rangle$ is the average of the transformation tensor, and $l_{\nu\alpha}$ is the cosine of the angle between the laboratory-frame axis $\nu=x,y,z$ and the molecular frame axis $\alpha=x,y,z$. These are universal quantities (see, e.g., Thirunamanchandran 1971) and the second-, third-, fourth-, and fifth-rank averaged $\mathbf{T}^{(s)}$ are

$$\langle \boldsymbol{a}_2^{\nu_2}\boldsymbol{a}_1^{\nu_1}\rangle = \frac{1}{3}\delta_{\nu_2\nu_1}\boldsymbol{a}_2\cdot\boldsymbol{a}_1, \tag{21}$$

and

$$\langle \boldsymbol{a}_3^{\nu_3}\boldsymbol{a}_2^{\nu_2}\boldsymbol{a}_1^{\nu_1}\rangle = \frac{1}{6}\epsilon_{\nu_3\nu_2\nu_1}\boldsymbol{a}_3\cdot(\boldsymbol{a}_2\times\boldsymbol{a}_1), \tag{22}$$

while for the fourth and fifth ranks we use Eq. (20) with

$$\mathbf{T}^{(4)}_{\nu_4\nu_3\nu_2\nu_1,\alpha_4\alpha_3\alpha_2\alpha_1} = \frac{1}{30}\begin{pmatrix} \delta_{\nu_4\nu_3}\delta_{\nu_2\nu_1} \\ \delta_{\nu_4\nu_2}\delta_{\nu_3\nu_1} \\ \delta_{\nu_4\nu_1}\delta_{\nu_3\nu_2}\end{pmatrix}^T \begin{pmatrix} 4 & -1 & -1 \\ -1 & 4 & -1 \\ -1 & -1 & 4\end{pmatrix} \begin{pmatrix} \delta_{\alpha_4\alpha_3}\delta_{\alpha_2\alpha_1} \\ \delta_{\alpha_4\alpha_2}\delta_{\alpha_3\alpha_1} \\ \delta_{\alpha_4\alpha_1}\delta_{\alpha_3\alpha_2}\end{pmatrix}, \tag{23}$$

and

$$\mathbf{T}^{(5)}_{\nu_5\nu_4\nu_3\nu_2\nu_1,\alpha_5\alpha_4\alpha_3\alpha_2\alpha_1} = \frac{1}{30}\begin{pmatrix} \epsilon_{\nu_5\nu_4\nu_3}\delta_{\nu_2\nu_1} \\ \epsilon_{\nu_5\nu_4\nu_2}\delta_{\nu_3\nu_1} \\ \epsilon_{\nu_5\nu_4\nu_1}\delta_{\nu_3\nu_2} \\ \epsilon_{\nu_5\nu_3\nu_2}\delta_{\nu_4\nu_1} \\ \epsilon_{\nu_5\nu_3\nu_1}\delta_{\nu_4\nu_2} \\ \epsilon_{\nu_5\nu_2\nu_1}\delta_{\nu_4\nu_3}\end{pmatrix}^T \begin{pmatrix} 3 & -1 & -1 & 1 & 1 & 0 \\ -1 & 3 & -1 & -1 & 0 & 1 \\ -1 & -1 & 3 & 0 & -1 & -1 \\ 1 & -1 & 0 & 3 & -1 & 1 \\ 1 & 0 & -1 & -1 & 3 & -1 \\ 0 & 1 & -1 & 1 & -1 & 3\end{pmatrix} \begin{pmatrix} \epsilon_{\alpha_5\alpha_4\alpha_3}\delta_{\alpha_2\alpha_1} \\ \epsilon_{\alpha_5\alpha_4\alpha_2}\delta_{\alpha_3\alpha_1} \\ \epsilon_{\alpha_5\alpha_4\alpha_1}\delta_{\alpha_3\alpha_2} \\ \epsilon_{\alpha_5\alpha_3\alpha_2}\delta_{\alpha_4\alpha_1} \\ \epsilon_{\alpha_5\alpha_3\alpha_1}\delta_{\alpha_4\alpha_2} \\ \epsilon_{\alpha_5\alpha_2\alpha_1}\delta_{\alpha_4\alpha_3}\end{pmatrix}. \tag{24}$$

The optical fields, wave vectors, and space coordinates are defined in the laboratory frame, while the transition dipoles and the positions of the chromophores are given in the molecular frame. The molecular susceptibilities need to be averaged over the relative orientation of the two frames. In Appendix B we give the required orientational averagings for nonlinear susceptibilities to the first order in the wave vector. Nonlinear susceptibilities and response functions can be calculated by combining these with Eqs. (20)–(24).

Using Eqs. (21)–(24) the nonvanishing tensor components can be predicted for each order in the field, both within and beyond the dipole approximation. $\chi^{(1)}$ in the dipole approximation only requires second-rank orientational averaging. This has one independent tensor component xx and the tensor is parity even, thus NC. To the first order in the wave vector we need either a second-rank (for magnetic dipole) or a third-rank (for the nonlocal contribution) tensor. A close look at the averaging properties of the following cross product: $(\mathbf{k}\times\boldsymbol{m})^{\nu}=\mathbf{k}^{\nu+1}\boldsymbol{m}^{\nu+2}-\mathbf{k}^{\nu+2}\boldsymbol{m}^{\nu+1}$, gives $\langle(\mathbf{k}\times\boldsymbol{m})^{\nu_2}\boldsymbol{\mu}^{\nu_1}\rangle = \mathbf{k}^{\nu_2+1}\langle\boldsymbol{m}^{\nu_2+2}\boldsymbol{\mu}^{\nu_1}\rangle - \mathbf{k}^{\nu_2+2}\langle\boldsymbol{m}^{\nu_2+1}\boldsymbol{\mu}^{\nu_1}\rangle$ which is equal to $\frac{1}{3}[\mathbf{k}^{\nu_2+1}\delta_{\nu_2+2,\nu_1}-\mathbf{k}^{\nu_2+2}\delta_{\nu_2+1,\nu_1}](\boldsymbol{m}\cdot\boldsymbol{\mu})$. Thus a nonzero contribution from $\langle(\mathbf{k}\times\boldsymbol{m})^{\nu_2}\boldsymbol{\mu}^{\nu_1}\rangle$ gives tensor components of type xy. The same components arise from the nonlocal contribution $(\mathbf{k}\cdot\mathbf{r})\mu\mu$ whose third-rank orientational averaging gives a tensor component of $(z)xy$ (see Table II). Thus, both contributions (nonlocal electric and magnetic) yield the same off

TABLE II. Nonvanishing tensor components of the macroscopic susecptibilities $\chi^{(1)} \equiv \langle \alpha \rangle$, $\chi^{(2)} \equiv \langle \beta \rangle$, and $\chi^{(3)} \equiv \langle \gamma \rangle$ in isotropic system to the zeroth and first orders in the wave vector. ν denotes the tensor components. Only independent tensor components are shown (permutations of x, y, and z give the same tensor elements).

Susceptibility	Zeroth order in **k** (the dipole approximation)	Parity	First order in **k**[a]	Parity
$\chi^{(1)}_{\nu_2\nu_1}$	xx	+	$(z)xy$	−
$\chi^{(2)}_{\nu_3\nu_2\nu_1}$	xyz	−	$(x)xyy$, $(x)yyx$, $(x)yxy$	+
$\chi^{(3)}_{\nu_4\nu_3\nu_2\nu_1}$	$xxyy$, $xyyx$, $xyxy$	+	$(z)xxxy$, $(z)xxyx$, $(z)xyxx$, $(z)zxyz$, $(z)zxzy$, $(z)zzxy$	−

[a]Vector component of **k** is given in brackets.

diagonal tensor components and are distinguishable from the diagonal tensor component which is the dipole approximation.

Using the same lines of argument we find that the second- and third-order nonlinear susceptibilities to the zeroth and first orders in the wave vector have the tensor components listed in Table II. Different orders in the wave vector are distinguishable and can be measured independently. The first- and the third-order signals linear in **k** and the second-order signals to the zeroth order in **k** are parity odd (CI).

The same reasoning applies when taking into account the charge-density contribution Q in Eq. (3). The electric current operator $\mathbb{J}$ is dominant in resonant techniques. The complete expressions for nonlinear signals with Q terms are given in Ref. 44. The complete NEEs with Q terms are used in Appendices C and E. For brevity, we will keep $Q=0$ in the main text.

Q does not contribute to the linear response since it involves $\mathbb{A}^2$. It also does not contribute to the time-domain experiments with well-separated pulses since we require each interaction to occur with a different pulse. Thus, Q can contribute only to second- and third-order responses in the frequency domain. In the second order $\beta \propto \mathrm{Tr}[\mathbb{J}(\tau_3)Q(\tau_2,\tau_1)\rho]$ (two simultaneous interactions correspond to Q, $\tau_2 \equiv \tau_1$); only g' terms are resonant in SFG. In the dipole approximation $\beta \propto \mu g'$. Its orientational averaging, however, vanishes since only μ is a molecular vector. To the first order in the wave vector, the magnetic field from $\mathbb{J}$ will not contribute [$\chi^{(2)}$ contains orientational averaging of one vector m]. Either $\mathbf{kr}\mu$ from $\mathbb{J}$ or $\mathbf{kr}g'$ from Q will yield the $(z)zxx$ tensor component, which is invariant to $\mathcal{P}$ and, thus, NC. The resonant DFG does not involve Q interactions. At the third order $\gamma \propto \mathrm{Tr}[\mathbb{J}(\tau_4)\mathbb{J}(\tau_3)Q(\tau_2,\tau_1)\rho]$; only g' and f' terms contribute. In the dipole approximation $\gamma \propto \mu\mu g'$ which yields a NC $zzxx$ tensor component. The CI components will contribute to the same tensor components as in Table II. Thus, the interaction terms involving Q do not affect the parity symmetry and the classification of Table II.

V. SURVEY OF NONLINEAR SIGNALS

The nonlinear optical response may be calculated as a sum over transitions between eigenstates.[42,46] This approach is, however, very expensive for large systems. Instead, calculations will be performed using the NEE. These were originally developed by Spano and Mukamel[47,48] for the third-order spectroscopy of aggregates made out of two-level chromophores, and later extended to three-level chromophores and semiconductors. The NEE attributes the nonlinear response to the scattering of quasiparticles (excitons) rather than to transitions among eigenstates. The quadratic dependence of $\hat{H}'$ on the exciton operators [Eq. (4)] provides another mechanism for nonlinearity. Since two-exciton resonances accessible by third-order nonlinear techniques originate from scattering, the costly calculation of two-exciton states is avoided. By taking into account the finite localization length of excitons and the short range of exciton-exciton interactions, the required computational time scales linearly with the size for large systems. Conventional sum-over-states-based methods scale at least cubically with the system size. The NEE is, therefore, particularly suitable for calculating the nonlinear optical response of extended structures.

Below we derive closed expressions for various nonlinear resonant techniques by invoking the RWA.

A. Linear techniques

In linear spectroscopy, phase matching simply implies that the signal propagates along the same direction of the incoming field. Only the $\mathbb{J}$ operator contributes to the linear response in Eq. (3). The linear-response function calculated in Appendix D [Eq. (D8)] and the corresponding susceptibility is

$$X^{(1)}_{\nu_S\nu_1}(-\mathbf{k}_S,-\omega_S,\mathbf{k}_1,\omega_1) = 2\pi\frac{i}{c}\delta(\omega_S-\omega_1)\sum_{\xi}\langle \boldsymbol{j}^{\nu_S}_{\xi}(-\mathbf{k}_2)\boldsymbol{j}^{*\nu_1}_{\xi}(-\mathbf{k}_1)\rangle I_{\xi}(\omega_1) + \text{c.c.}'. \tag{25}$$

Here $\boldsymbol{j}_{\xi}(\mathbf{k}) \equiv \Sigma_n \psi_{\xi n}\exp(i\mathbf{kr}_n)\boldsymbol{j}_n$ and c.c.′ denotes the complex conjugate with changing the signs of all the frequencies and wave vectors. $X^{(1)}$ may be used to calculate linear signals: absorption (zero order in the wave vector) and CD (first order).

The absorption signal σ_A is obtained in the dipole approximation ($\mathbf{k}=0$) and is related to the imaginary part of the response function. It measures the change in the intensity of the transmitted light with respect to the incoming light [Eq. (22) in Ref. 37]. Thus, no polarization-related property is involved and

$$\sigma_A(\omega) \propto \mathrm{Im}\,\chi^{(1)} = \frac{c}{\omega^2}\,\mathrm{Im}\,X^{(1)}_{xx}(-\omega,\omega)$$

$$\propto \frac{1}{\omega^2}\sum_{\xi}\frac{\gamma_\xi |\boldsymbol{j}_\xi|^2}{(\omega - E_\xi)^2 + \gamma_\xi^2},$$

where E_ξ is the energy of exciton ξ and γ_ξ is its dephasing rate. We note that to the zero order in the wave vector and in the RWA $\boldsymbol{j}_\xi = -i\omega\boldsymbol{\mu}_l$.

The CD signal is defined as the difference between the absorption of left and right circularly polarized light and is given by Eq. (23) in Ref. 37, which does not assume any specific form for the susceptibility. Using $\chi^{(1)}(-\mathbf{k}_S - \omega_s; \mathbf{k}\omega) = (c/\omega_S\omega_1)X^{(1)}(-\mathbf{k}_S - \omega_s; \mathbf{k}\omega)$ and expanding the current to first order in the wave vector, $\boldsymbol{j}_l(\mathbf{k}) \approx -i\omega\boldsymbol{\mu}_l - \omega(\mathbf{k}\cdot\mathbf{r}_l)\boldsymbol{\mu}_l + i\mathbf{k}\times\boldsymbol{m}_l$, we obtain

$$\sigma_{\mathrm{CD}}(\omega) \propto \frac{1}{\lambda}\sum_{\xi}\frac{\gamma_\xi \rho_\xi}{(\omega - E_\xi)^2 + \gamma_\xi^2},$$

where $\lambda = 2\pi c/\omega$ is the wavelength, $\mathbf{r}_{ll'} = \mathbf{r}_l - \mathbf{r}_{l'}$, and $\rho_\xi \equiv \Sigma_{ll'}\psi_{\xi l}\psi_{\xi l'}[\mathbf{r}_{ll'}\cdot(\mu_l \times \mu_{l'}) - 2\Im\mu_l \boldsymbol{m}_{l'}]$ is known as the rotational strength. This expression coincides with the matrix method widely used for calculating CD in peptides and proteins.[49,50]

B. Second-order techniques

By isotropic symmetry, second-harmonic generation is forbidden in liquids.[51,52] However, the first hyperpolarizability (second-order susceptibility) β does not vanish identically. Second-order coherent signals have been observed in a noncollinear pulse configuration in chiral liquids[20,53,54] followed by calculations.[19,21,55]

Both frequency- and time-domain SFG/DFG techniques are commonly used to study the structure and dynamics at interfaces and surfaces.[56–62] Frequency-domain techniques which measure the signal with a frequency of $\omega_1 + \omega_2$ (SFG) or $\omega_1 - \omega_2$ (DFG) give equilibrium surface properties. The incoming frequencies ω_1, ω_2, and the signal frequency can be tuned to specific electronic and vibrational resonances. Ultrashort time-domain techniques monitor the time evolution of vibrational and electronic coherences and their variation with the time delay between pulses.[60] Time-domain SFG and DFG techniques probe doubly excited and singly excited states, respectively, including exciton coherence, interactions, and dephasing[60,63,64] and may be used to monitor dynamical processes such as protein folding.

Observing second-order techniques in liquids requires special experimental conditions.[18] This is because the response function includes the Levi-Cività tensor $\epsilon_{\nu_3\nu_2\nu_1}$ which relates the direction $\nu_3 = x, y, z$ of the induced electric field with two incoming orthogonal electric fields, ν_2 and ν_1 [see Eq. (22)]. Obviously this cannot be satisfied by phase-matched transverse optical fields generated along $\mathbf{k}_S = \mathbf{k}_1 \pm \mathbf{k}_2$. Thus, the signal must have a phase mismatch either in direction or in the wave-vector magnitude.

Below we calculate $\chi^{(2)}$ to first order in $\mathbf{k}$.[37] We consider techniques where both the incoming field frequencies (ω_1 and ω_2) are resonant with the one-exciton transitions $\bar{\Omega}$. The Feynman diagrams and the corresponding scattering pathways are shown in Fig. 2.

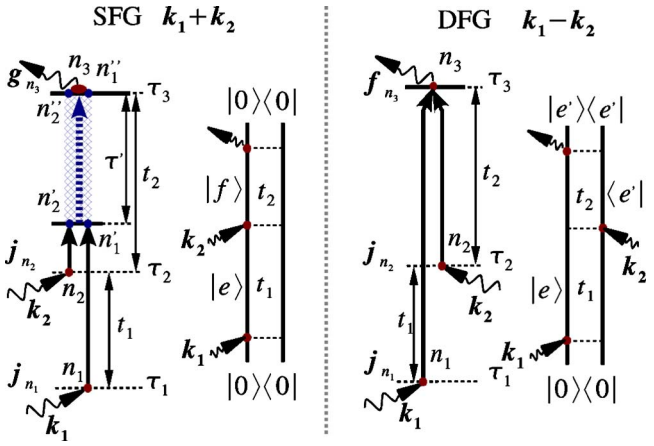

FIG. 2. Feynman diagrams and the corresponding scattering pathways (Ref. 36) for second-order sum frequency generation (SFG) and difference frequency generation (DFG) signals. DFG does not involve two-exciton resonances and is, thus, independent on exciton scattering.

1. Frequency-domain techniques

We first consider a SFG signal propagating along $\mathbf{n}_S = (\mathbf{n}_1 + \mathbf{n}_2)/|\mathbf{n}_1 + \mathbf{n}_2|$. We assume monochromatic optical fields [Eq. (13)] where the signal frequency $\omega_S = \omega_1 + \omega_2$ is close to a two-exciton resonance. The second-order SFG susceptibility within the RWA X^{SFG} is calculated by solving the NEE in Appendix F. The final result in the exciton basis reads

$$X^{\mathrm{SFG}}_{\nu_S\nu_2\nu_1}(-\mathbf{k}_S, -\omega_S, \mathbf{k}_2, \omega_2, \mathbf{k}_1, \omega_1)$$
$$= 2\pi\frac{i^2}{c^2}\delta(\omega_S - \omega_2 - \omega_1)$$
$$\times \sum_{\mathrm{perm}_2}\sum_{\xi_4\xi_3\xi_2\xi_1}[2\langle \boldsymbol{g}^{\nu_S}_{\xi_4\xi_3}(-\mathbf{k}_S)\boldsymbol{j}^{*\nu_2}_{\xi_2}(-\mathbf{k}_2)\boldsymbol{j}^{*\nu_1}_{\xi_1}(-\mathbf{k}_1)\rangle$$
$$\times D^{-1}_{\xi_4\xi_3\xi_2\xi_1}(\omega_2 + \omega_1)\mathcal{I}_{\xi_2\xi_1}(\omega_2 + \omega_1)I_{\xi_1}(\omega_1) + \mathrm{c.c.}'], \tag{26}$$

Here ξ denotes one-exciton eigenstates, $\boldsymbol{g}_{\xi_2\xi_1}(\mathbf{k}) \equiv \Sigma_n \psi_{\xi_2 n}\psi_{\xi_1 n}\exp(i\mathbf{k}\mathbf{r}_n)\boldsymbol{g}_n$ and $\boldsymbol{j}_\xi(\mathbf{k}) \equiv \Sigma_n \psi_{\xi n}\exp(i\mathbf{k}\mathbf{r}_n)\boldsymbol{j}_n$ are the corresponding transition amplitudes in the one-exciton basis, and ψ_ξ are the eigenfunctions of the one-exciton Hamiltonian obtained from Eq. (2). $I_\xi(\omega)$ is the one-exciton Green's function [Eq. (D5)], $\mathcal{I}_{\xi\xi'}(\omega)$ is the Green's function of the noninteracting exciton pair [Eq. (F7)], and $D^{-1}(\omega)$ is related to the two-exciton scattering matrix $\Gamma(\omega)$ by Eq. (F8). The transformation of these matrices between basis sets is defined by Eq. (F12).

We next turn to DFG where the signal frequency $\omega_S \ll \bar{\Omega}$ is resonant with the transitions within the one-exciton band and the signal propagates along $\mathbf{n}_S = (\mathbf{n}_1 - \mathbf{n}_2)/|\mathbf{n}_1 - \mathbf{n}_2|$. The DFG susceptibility is calculated in Appendix F. Transforming Eq. (F16) to the exciton basis leads to

$$X^{\mathrm{DFG}}_{\nu_S\nu_2\nu_1}(-\mathbf{k}_S,-\omega_S,-\mathbf{k}_2,-\omega_2,\mathbf{k}_1,\omega_1)$$
$$=-2\pi\frac{i^2}{c^2}\delta(\omega_S+\omega_2-\omega_1)$$
$$\times\sum_{\mathrm{perm}_2}\sum_{\xi_2\xi_1}\langle f^{\nu_S}_{\xi_2\xi_1}(-\mathbf{k}_S)j^{\nu_2}_{\xi_2}(-\mathbf{k}_2)j^{*\nu_1}_{\xi_1}(-\mathbf{k}_1)\rangle$$
$$\times I^*_{\xi_2}(\omega_2)I_{\xi_1}(\omega_1), \tag{27}$$

where $\boldsymbol{j}_\xi(\mathbf{k})$ is the exciton transition current, $\boldsymbol{f}_{\xi_2\xi_1}(\mathbf{k})\equiv\Sigma_n\psi_{\xi_2 n}\psi_{\xi_1 n}\exp(i\mathbf{k}\mathbf{r}_n)\boldsymbol{f}_n$ is the permanent current in the exciton basis, and $I_\xi(\omega)$ is the one-exciton Green's function. We note that this technique depends on permanent dipoles and does not show two-exciton resonances.

2. Time-domain techniques

We first consider SFG where the signal is generated along $\mathbf{n}_S=(\mathbf{n}_1+\mathbf{n}_2)/|\mathbf{n}_1+\mathbf{n}_2|$ with wave vector $\mathbf{k}_S=(\omega_S/c)\mathbf{n}_S$ and frequency $\omega_S=\omega_1+\omega_2$ close to the two-exciton resonance $2\bar{\Omega}$. Using Eq. (F10) and following the procedure used in Sec. V B 1 we express the response in terms of one-exciton Green's functions,

$$\mathbb{R}^{\mathrm{SFG}}_{\nu_S\nu_2\nu_1}(\mathbf{k}_S,\mathbf{k}_2,\mathbf{k}_1;\Omega_2,\Omega_1)$$
$$=2\frac{i^2}{c^2}\sum_{\xi_4\xi_3\xi_2\xi_1}\langle g^{\nu_S}_{\xi_4\xi_3}(-\mathbf{k}_1-\mathbf{k}_2)j^{*\nu_2}_{\xi_2}(-\mathbf{k}_2)j^{*\nu_1}_{\xi_1}(-\mathbf{k}_1)\rangle$$
$$\times D^{-1}_{\xi_4\xi_3\xi_2\xi_1}(\Omega_2)\mathcal{I}_{\xi_2\xi_1}(\Omega_2)I_{\xi_1}(\Omega_1), \tag{28}$$

where Ω_1 and Ω_2 are the frequency transform conjugates to the time intervals $t_1\equiv\tau_2-\tau_1$ and $t_2\equiv\tau_3-\tau_2$. Ω_2 shows the two-exciton resonances. g' does not enter into this signal since we assume well-separated pulses.

DFG is generated along $\mathbf{n}_S=(\mathbf{n}_1-\mathbf{n}_2)/|\mathbf{n}_1-\mathbf{n}_2|$ where the signal frequency $\omega_S=\omega_1-\omega_2$ is then resonant with the transitions within the one-exciton band. This signal is obtained from Eq. (F15) which in exciton basis gives

$$\mathbb{R}^{\mathrm{DFG}}_{\nu_S\nu_2\nu_1}(\mathbf{k}_S,\mathbf{k}_2,\mathbf{k}_1;\Omega_2,\Omega_1)$$
$$=-2\frac{i^2}{c^2}\sum_{\xi_2\xi_1}\langle f^{\nu_S}_{\xi_2\xi_1}(-\mathbf{k}_1-\mathbf{k}_2)j^{\nu_2}_{\xi_2}(-\mathbf{k}_2)j^{*\nu_1}_{\xi_1}(-\mathbf{k}_1)\rangle$$
$$\times I^*_{\xi_2}(-\Omega_2)I_{\xi_1}(\Omega_1). \tag{29}$$

This signal measures exciton coherence and population dynamics.

C. Third-order techniques

Most commonly used ultrafast techniques such as transient grating, photon echo, pump probe, and resonance Raman are third order. The pump probe and transient grating are used to track exciton populations, transport as well as to follow charge separation and recombination. Coherent techniques such as the photon echo can discriminate between homogeneous and inhomogeneous contributions to line shapes of highly congested spectra. Vibrational nonlinear optical techniques were recently applied to protein structure determination and folding dynamics[65] and hydrogen bonding in water.[66] The Resonance Raman techniques probe vibrational transitions coupled to specific electronic resonances.[67]

The third-order response of excitons is usually calculated by invoking the dipole, $\mathbf{k}=0$, approximation. The possibility to use the third-order signals (which unlike the second order does not suffer from phase-matching problems) to the first order in the wave vector opens up numerous exciting new possibilities. The signal frequency within the RWA is $\omega_S=\pm\omega_3\pm\omega_2\pm\omega_1$ and the signal is measured along $\mathbf{n}_S=(\pm\mathbf{n}_3\pm\mathbf{n}_2\pm\mathbf{n}_1)/|\pm\mathbf{n}_3\pm\mathbf{n}_2\pm\mathbf{n}_1|$. Below we assume one-color signals where $\omega_1\approx\omega_2\approx\omega_3\approx\bar{\Omega}$ with complete phase matching. This gives one frequency-domain signal $\mathbf{k}_S=\mathbf{k}_1+\mathbf{k}_2-\mathbf{k}_3$ and three independent signals $\mathbf{k}_\mathrm{I}=-\mathbf{k}_1+\mathbf{k}_2+\mathbf{k}_3$, $\mathbf{k}_\mathrm{II}=\mathbf{k}_1-\mathbf{k}_2+\mathbf{k}_3$, and $\mathbf{k}_\mathrm{III}=\mathbf{k}_1+\mathbf{k}_2-\mathbf{k}_3$ in the time domain.

The response function and the susceptibility for different third-order signals have been calculated in Refs. 36–38 by ignoring local magnetic dipoles using the Green's-function solution of the NEE. Below we generalize these expressions using transition currents to the first order in $\mathbf{k}$.

1. Frequency-domain techniques

The third-order susceptibility for $\mathbf{k}_S=\mathbf{k}_1+\mathbf{k}_2-\mathbf{k}_3$ is

$$X^{(3)}_{\nu_S,\nu_3\nu_2\nu_1}(-\mathbf{k}_S,-\omega_S;-\mathbf{k}_3,-\omega_3,\mathbf{k}_2,\omega_2,\mathbf{k}_1,\omega_1)$$
$$=2\pi\frac{i^3}{c^3}\delta(\omega_S+\omega_3-\omega_2-\omega_1)$$
$$\times\sum_{\mathrm{perm}}\sum_{\xi_4\xi_3\xi_2\xi_1}\langle j^{\nu_S}_{\xi_4}(-\mathbf{k}_S)j^{\nu_3}_{\xi_3}(-\mathbf{k}_3)j^{\nu_2*}_{\xi_2}(-\mathbf{k}_2)j^{\nu_1*}_{\xi_1}(-\mathbf{k}_1)\rangle$$
$$\times\Gamma_{\xi_4\xi_3,\xi_2\xi_1}(\omega_2+\omega_1)I_{\xi_4}(\omega_4)I^*_{\xi_3}(\omega_3)I_{\xi_2}(\omega_2)I_{\xi_1}(\omega_1)$$
$$+\mathrm{c.c.}'. \tag{30}$$

Various sections of this multiparameter function can be displayed. For example, we can assume $\omega_3=\omega_1$ and choose ω_2 and ω_1 as independent variables. The wave-vector configurations allow also the selection of various tensor components.

2. Time-domain techniques

We first consider $\mathbf{k}_1=-\mathbf{k}_1+\mathbf{k}_2+\mathbf{k}_3$, hold the second delay time fixed, and perform one-sided Fourier transforms with respect to t_1 and t_2. The frequency conjugates are denoted Ω_1 and Ω_2. The response denotes function is then given by:

$$\mathbb{R}^{\mathbf{k}_\mathrm{I}}_{\nu_S\nu_3\nu_2\nu_1}(\Omega_3,t_2,\Omega_1)$$
$$=-2\frac{i^3}{c^3}\sum_{\xi_4\cdots\xi_1}\langle j^{\nu_S}_{\xi_4}(+\mathbf{k}_1-\mathbf{k}_2-\mathbf{k}_3)j^{*\nu_3}_{\xi_3}(-\mathbf{k}_3)j^{*\nu_2}_{\xi_2}(-\mathbf{k}_2)$$
$$\times j^{\nu_1}_{\xi_1}(-\mathbf{k}_1)\rangle I^*_{\xi_1}(t_2)I_{\xi_2}(t_2)I^*_{\xi_1}(-\Omega_1)I_{\xi_4}(\Omega_3)$$
$$\times\Gamma_{\xi_4\xi_1\xi_3\xi_2}(\Omega_3+E_{\xi_1}+i\gamma_{\xi_1})\mathcal{I}_{\xi_3\xi_2}(\Omega_3+E_{\xi_1}+i\gamma_{\xi_1}). \tag{31}$$

For $\mathbf{k}_\mathrm{II}=\mathbf{k}_1-\mathbf{k}_2+\mathbf{k}_3$ we similarly get

$$\mathbb{R}^{\mathbf{k}_{\mathrm{II}}}_{\nu_S\nu_3\nu_2\nu_1}(\Omega_3,t_2,\Omega_1)$$
$$=-2\frac{i^3}{c^3}\sum_{\xi_4\cdots\xi_1}\langle \boldsymbol{j}^{\nu_S}_{\xi_4}(-\mathbf{k}_1+\mathbf{k}_2-\mathbf{k}_3)\boldsymbol{j}^{*\nu_3}_{\xi_3}(-\mathbf{k}_3)\boldsymbol{j}^{\nu_2}_{\xi_2}(-\mathbf{k}_2)$$
$$\times\boldsymbol{j}^{*\nu_1}_{\xi_1}(-\mathbf{k}_1)\rangle I^{*}_{\xi_2}(t_2)I_{\xi_1}(t_2)I_{\xi_1}(\Omega_1)I_{\xi_4}(\Omega_3)$$
$$\times\Gamma_{\xi_4\xi_2,\xi_3\xi_1}(\Omega_3+E_{\xi_2}+i\gamma_{\xi_2})\mathcal{I}_{\xi_3\xi_1}(\Omega_3+E_{\xi_2}+i\gamma_{\xi_2}). \quad (32)$$

or $\mathbf{k}_{\mathrm{III}}=\mathbf{k}_1+\mathbf{k}_2-\mathbf{k}_3$ we hold t_1 fixed and perform Fourier transforms with respect to t_2 and t_3 with the frequency conjugates Ω_2 and Ω_3. This gives

$$\mathbb{R}^{\mathbf{k}_{\mathrm{III}}}_{\nu_S\nu_3\nu_2\nu_1}(\Omega_3,\Omega_2,t_1)$$
$$=-2\frac{i^3}{c^3}\sum_{\xi_4\cdots\xi_1}\langle \boldsymbol{j}^{\nu_4}_{\xi_4}(-\mathbf{k}_1-\mathbf{k}_2+\mathbf{k}_3)\boldsymbol{j}^{\nu_3}_{\xi_3}(-\mathbf{k}_3)\boldsymbol{j}^{*\nu_2}_{\xi_2}(-\mathbf{k}_2)$$
$$\times\boldsymbol{j}^{*\nu_1}_{\xi_1}(-\mathbf{k}_1)\rangle I_{\xi_1}(t_1)I_{\xi_4}(\Omega_3)I^{*}_{\xi_3}(\Omega_2-\Omega_3)$$
$$\times[\Gamma_{\xi_4\xi_3,\xi_2\xi_1}(\Omega_2)\mathcal{I}_{\xi_2\xi_1}(\Omega_2)$$
$$-\Gamma_{\xi_4\xi_3,\xi_2\xi_1}(\Omega_3+E_{\xi_3}+i\gamma_{\xi_3})\mathcal{I}_{\xi_2\xi_1}(\Omega_3+E_{\xi_3}+i\gamma_{\xi 3})]. \quad (33)$$

VI. DISCUSSION

We have derived closed expressions for the lowest three optical susceptibilities to first order in the optical wave vector. For isotropic systems we find CI signals: $\chi^{(1)}$ and $\chi^{(3)}$ to first order in the wave vector and $\chi^{(2)}$ to zero order in the wave vector. Each tensor component can be classified as either CI- or NC-type.

Nonlinear optical signals show multiexciton resonances. Extracting the structural and dynamical information from these signals is a major challenge. Resonant techniques simplify the analysis since specific wave vector and polarization configurations can select few dominant peaks in each case.

Nonlinear techniques open up a broader range of possibilities for examining chirality, compared with linear techniques such as CD and ROA. Linear combinations of various tensor components can be measured and CI signals may be unambigously distinguished using the specific configurations of incoming fields.

Two-dimensional correlation plots of second-order signals, SFG and DFG, in the dipole approximation are very promising for the structure determination of proteins. Unlike the photon echo, second-order techniques do not eliminate inhomogeneous broadening, however, they involve fewer excitonic resonances and are less congested. Diagonal peaks in two-dimensional photon echoes are related to the fundamental one-exciton transitions. Several experimental techniques are used to eliminate these peaks and often resolve cross-peaks coming from couplings between chromophores.[14] Two-dimensional SFG and DFG techniques are different: Due to frequency permutation symmetry all diagonal peaks vanish in liquids. Off diagonal regions which carry additional information about structure and dynamics are therefore better resolved. The studies of these signals are our future direction.

We have simulated the linear absorption, CD, and third-order frequency- and time-domain signals. The application to the amide I IR band shows a large difference between the parallel and antiparallel β sheets, which are typical but hard to resolve structural motiffs of proteins. The parameters of the Hamiltonians were taken from Ref. 68 We have neglected the local magnetic dipoles $\boldsymbol{m}$.

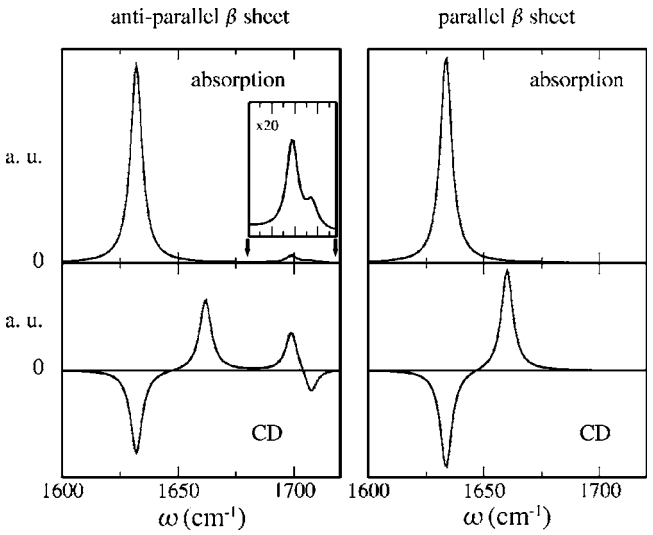

FIG. 3. Linear absorption (dipole approximation) and circular dichroism (first order in wave vector) of an ideal infinite antiparallel and a parallel β sheet in the amide I region.

The linear absorption and the CD of the two types of sheets are presented in Fig. 3. The linear absorption shows one major peak for both sheets. The higher energy peaks of the antiparallel β sheet are much weaker. The CD of the parallel β sheet shows sigmoidal line shape with a negative lobe at 1634 cm^{-1} and a positive lobe shifted by 20 cm^{-1} to higher frequency. The antiparallel β sheet shows four transitions in the CD originating from the four chromophores per unit cell.[34] This is very different from the absorption where only one strong peak is visible.

Both sheets show the CI third-order frequency domain signal $X^{(3)}_{\nu_4\nu_3\nu_2\nu_1}(-\omega_2,-\omega_1,\omega_2,\omega_1)$ with $\mathbf{k}_S=\mathbf{k}_1+\mathbf{k}_2-\mathbf{k}_3$, which is displayed in Fig. 4. Different off diagonal regions are amplified in the *xxxy* and *xxyx* tensor components. Diagonal peaks can be completely eliminated by combining these components. The different cross sections of the imaginary absorptive part of the two-dimensional (2D) plots show a complicated structure, which is different for the two sheets (see Fig. 5): The antiparallel β sheet has peaks at 1700 cm^{-1} which are absent in the parallel β sheet.

The difference is more pronounced in the time-domain $\mathbf{k}_1=-\mathbf{k}_1+\mathbf{k}_2+\mathbf{k}_3$ (photon echo) signal. The 2D plots are shown in Fig. 6 and the cross sections of the imaginary part are given in Fig. 7. The off diagonal region is much stronger than the diagonal $\omega_3=-\omega_1$ line. The *xxxy* tensor is asymmetric with respect to the diagonal and *xxyx* is symmetric. The cross sections show peaks with opposite signs for the two β sheets. This difference is missed in the absolute value 2D plots. Thus, measuring the phase profile is crucial for resolving the two structures.

Third-order CI signals amplify the off diagonal regions of the two-dimensional plots since such peaks are related to the couplings between chromophores. To the first order in the

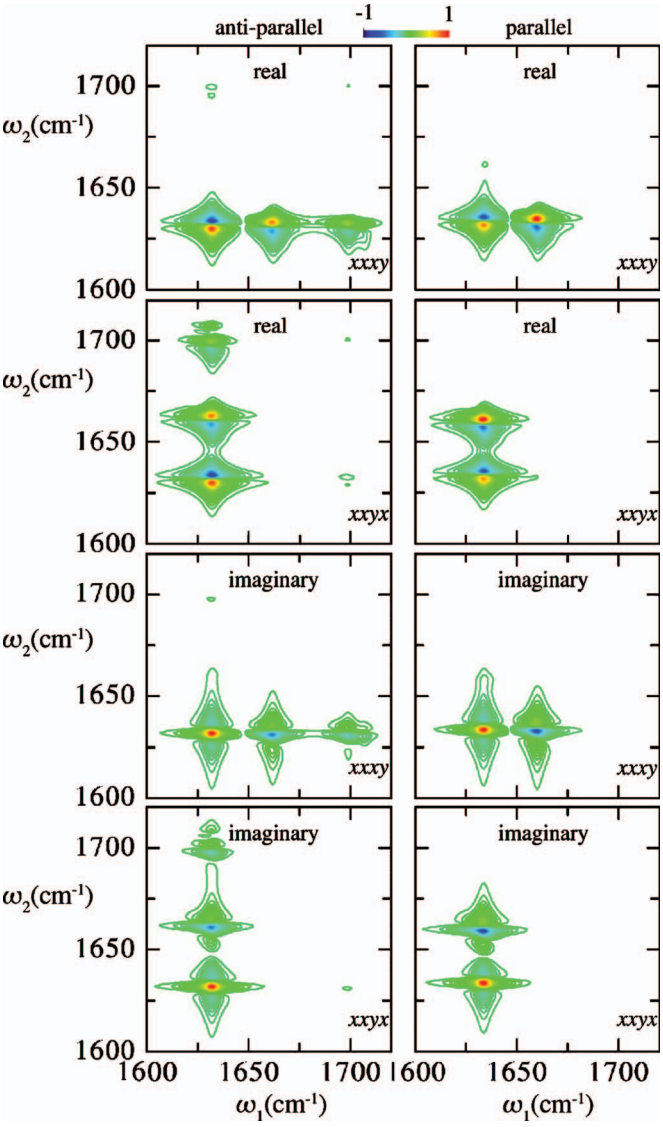

FIG. 4. (Color) Nonlinear third-order frequency-domain four-wave-mixing $[X^{(3)}_{\nu_4\nu_3\nu_2\nu_1}(-\omega_2,-\omega_1,\omega_2,\omega_1)]$ signals at $\mathbf{k}_1+\mathbf{k}_2-\mathbf{k}_3$ [Eq. (30)].

wave vector, the signals probe nonlocal system properties which are directly connected to these couplings. The nonlinear signals, therefore, are very sensitive to the couplings.

The CD which only shows one-exciton transitions has a slightly different pattern for the two sheets which can be used to distinguish between them. The third-order techniques provide a much more different characteristic pattern for the two sheets. Magnetic transition dipoles as well as the Q interaction elements, which were neglected in these simulations, can make corrections to the CD and third-order techniques.

Coherent control techniques can manipulate the signals and highlight their specific components.[69–73] Desired peaks can be selected and others can be eliminated. Many parameters, optical frequencies, phases, wave vector directions, and polarizations can be controlled in third-order frequency-domain spectroscopies. In ideal time-domain experiments time delays can be directly manipulated. Pulse shaping can give an intermediate regime between frequency- and time-domain experiments. With pulse shaping, various Liouville

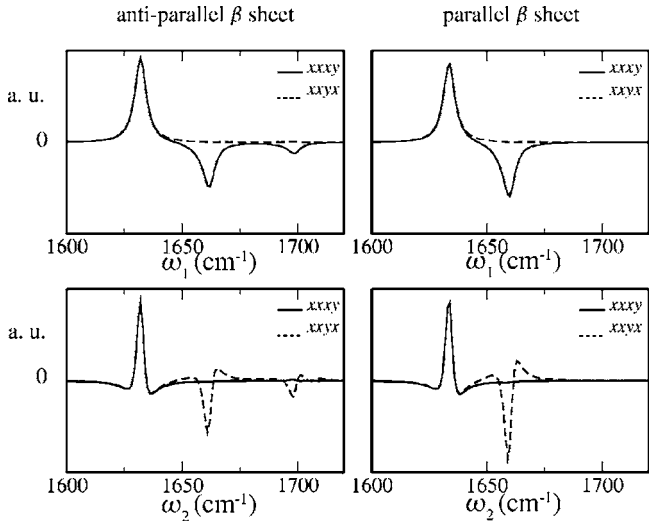

FIG. 5. Sections of the imaginary part of $X^{(3)}_{\nu_4\nu_3\nu_2\nu_1}(-\omega_2,-\omega_1,\omega_2,\omega_1)$ shown in Fig. 4. Top: Horizontal sections; for the antiparallel β sheet we used $\omega_2=1632$ cm^{-1}, and for the parallel $\omega_2=1634$ cm^{-1}, which corresponds to the maximum of linear absorption. Bottom: Vertical sections; $\omega_1=1632$ cm^{-1} for the antiparallel β sheet, and $\omega_1=1634$ cm^{-1} for the parallel.

space pathways are mixed and the signals contain their multiple interferences. Pulse polarization control is an exciting new development. Understanding the symmetries of nonlinear response functions and developing methods for the calculation of all the tensor components are required ingredients for polarization-sensitive experiments.

ACKNOWLEDGMENTS

This material is based upon the work supported by the National Science Foundation Grant No. CHE-0446555 and the National Institute of Health Grant No. 2 RO1 GM59230-05. This support is gratefully acknowledged. We also wish to thank Professor R. W. Woody for sharing his data.

APPENDIX A: THE MINIMAL-COUPLING INTERACTION HAMILTONIAN

Using the minimal-coupling Hamiltonian, the interaction of a system of point charges with the electromagnetic field is given by[40,41]

$$\hat{H}'(t)=\sum_\alpha \frac{-q_\alpha}{cm_\alpha}\hat{\mathbf{p}}_\alpha(t)\cdot\hat{\mathbb{A}}(\mathbf{r}_\alpha,t)+\frac{q_\alpha^2}{2m_\alpha c^2}\hat{\mathbb{A}}^2(\mathbf{r}_\alpha,t), \qquad \text{(A1)}$$

where Σ_α runs over all charges q_α with masses m_α, and $\hat{\mathbb{A}}$ is the vector potential of the field. This interaction Hamiltonian can be recast using electric current and charge-density operators. The current operator is $\hat{\mathbb{J}}(\mathbf{r},t)=\Sigma_\alpha(q_\alpha\hbar/2m_\alpha i)\times[\hat{\varphi}^\dagger_\alpha(\mathbf{r},t)\nabla\hat{\varphi}_\alpha(\mathbf{r},t)-(\nabla\hat{\varphi}^\dagger_\alpha(\mathbf{r},t))\hat{\varphi}_\alpha(\mathbf{r},t)]$ and we define the operator $Q(\mathbf{r},t)=-\Sigma_\alpha(q_\alpha/2m_\alpha c)\hat{\sigma}_\alpha(\mathbf{r},t)$ related to the charge density $\hat{\sigma}_\alpha(\mathbf{r},t)=q_\alpha\hat{\varphi}^\dagger_\alpha(\mathbf{r},t)\hat{\varphi}_\alpha(\mathbf{r},t)$ [where $\hat{\varphi}_\alpha(\mathbf{r},t)$ is the field operator for particle α]. We then get

$$\hat{H}'(t)=-\frac{1}{c}\int d\mathbf{r}[\hat{\mathbb{J}}(\mathbf{r},t)\cdot\hat{\mathbb{A}}(\mathbf{r},t)+Q(\mathbf{r},t)\hat{\mathbb{A}}^2(\mathbf{r},t)]. \qquad \text{(A2)}$$

The Frenkel exciton model is defined by the localized (nonoverlapping) basis set of isolated chromophores $\phi_l(m)$,

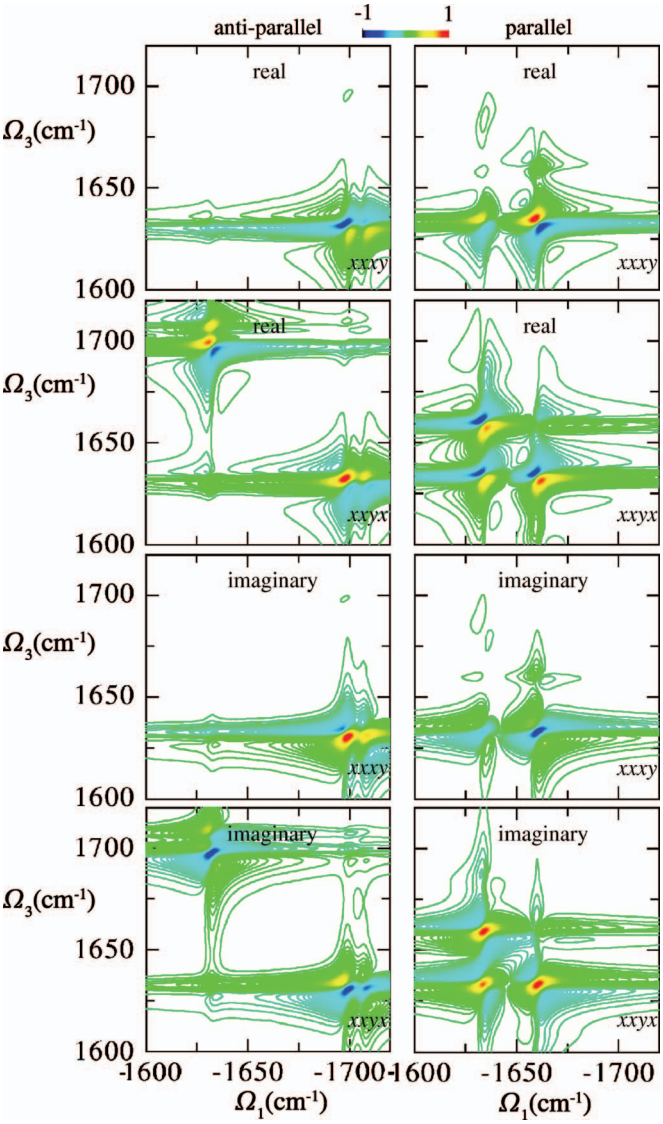

FIG. 6. (Color) Nonlinear third-order time-domain four-wave-mixing $[\mathbb{R}^{\mathbf{k}_I}_{\nu_4\nu_3\nu_2\nu_1}(\Omega_3,t_2=0,\Omega_1)$ in Eq. (31)] signals for $\mathbf{k}_I=-\mathbf{k}_1+\mathbf{k}_2+\mathbf{k}_3$.

where l is the state of chromophore m. We then obtain Eqs. (4) and (5) for the current and charge-density operators for the entire aggregates where

$$\boldsymbol{j}_m \equiv \int d\mathbf{r}\,\phi_e^\dagger(m)\hat{\mathbb{J}}(\mathbf{r},t)\phi_g(m),$$

$$\boldsymbol{f}_m \equiv \int d\mathbf{r}\,\phi_e^\dagger(m)\hat{\mathbb{J}}(\mathbf{r},t)\phi_e(m),$$

and

$$\boldsymbol{g}_m \equiv \int d\mathbf{r}\,\phi_{2e}^\dagger(m)\hat{\mathbb{J}}(\mathbf{r},t)\phi_g(m)$$

and

$$j'_m \equiv \int d\mathbf{r}\,\phi_e^\dagger(m)Q(\mathbf{r},t)\phi_g(m),$$

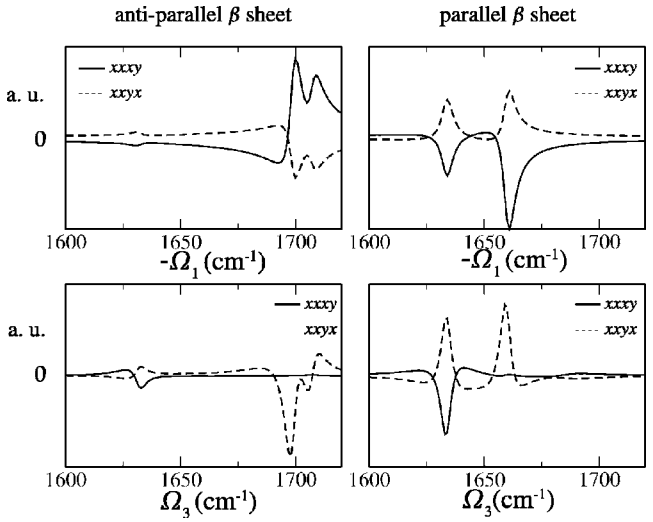

FIG. 7. Sections of the imaginary part of $\mathbb{R}^{\mathbf{k}_I}_{\nu_4\nu_3\nu_2\nu_1}(\Omega_3,t_2=0,\Omega_1)$ shown in Fig. 6. Top: Horizontal sections; for the antiparallel β sheet we used $\Omega_3=1632\ \mathrm{cm}^{-1}$, and for the parallel $\Omega_3=1634\ \mathrm{cm}^{-1}$. Bottom: Vertical sections; $\Omega_1=-1632\ \mathrm{cm}^{-1}$ for the antiparallel β sheet, and $\Omega_1=-1634\ \mathrm{cm}^{-1}$ for the parallel.

$$f'_m \equiv \int d\mathbf{r}\,\phi_e^\dagger(m)Q(\mathbf{r},t)\phi_e(m),$$

and

$$g'_m \equiv \int d\mathbf{r}\,\phi_{2e}^\dagger(m)Q(\mathbf{r},t)\phi_g(m);$$

$\phi_g(m)$ denotes the ground state of the mth chromophore, $\phi_e(m)$ its excited state, and $\phi_{2e}(m)$ its overtone. Thus, each chromophore is treated as a point particle with its own transition currents.

$\hat{\mathbb{J}}(\mathbf{r})$ can be alternatively expressed in terms of the electric polarization, $\hat{\mathbf{P}}(\mathbf{r},t)$, and magnetization, $\hat{\mathbf{M}}(\mathbf{r},t)$, operators,

$$\hat{\mathbb{J}}(\mathbf{r},t)=\frac{\partial}{\partial t}\hat{\mathbf{P}}(\mathbf{r},t)+\nabla\times\hat{\mathbf{M}}(\mathbf{r},t), \tag{A3}$$

where $\hat{\mathbf{P}}$ is responsible for the longitudinal charge displacements and $\hat{\mathbf{M}}$ to the circular displacement giving rise to angular momentum. This relation is considerably simplified in the $\mathbf{k}\omega$ domain $[F(\mathbf{r}t)=[1/(2\pi)^4]\int d\mathbf{k}\int d\omega F(\mathbf{k}\omega)e^{i\mathbf{k}\mathbf{r}-i\omega t}]$,

$$\hat{\mathbb{J}}(\mathbf{k}\omega)=-i\omega\hat{\mathbf{P}}(\mathbf{k}\omega)+i\mathbf{k}\times\hat{\mathbf{M}}(\mathbf{k}\omega). \tag{A4}$$

The polarization and the magnetization operators for excitons in the $\mathbf{k}\omega$ domain are given by

$$\hat{\mathbf{P}}(\mathbf{k},\omega)=\sum_l \exp(-i\mathbf{k}\mathbf{r}_l)\{\boldsymbol{\mu}_l(\hat{B}_l^\dagger(\omega)+\hat{B}_l(\omega)) + \boldsymbol{\mu}'_l\hat{B}_l^\dagger(\omega)\hat{B}_l(\omega)+\boldsymbol{\mu}''_l(\hat{B}_l^{\dagger 2}(\omega)+\hat{B}_l^2(\omega))\}, \tag{A5}$$

$$\hat{\mathbf{M}}(\mathbf{k},\omega)=\sum_l \exp(-i\mathbf{k}\mathbf{r}_l)\{\boldsymbol{m}_l^*\hat{B}_l^\dagger(\omega)+\boldsymbol{m}_l\hat{B}_l(\omega) + \boldsymbol{m}_l'\hat{B}_l^\dagger(\omega)\hat{B}_l(\omega)+\boldsymbol{m}_l''^*\hat{B}_l^{\dagger 2}(\omega)+\boldsymbol{m}_l''tB_l^2(\omega)\}, \tag{A6}$$

where the sum runs over all chromophores, $\hat{B}_l^\dagger(\omega)=\int dt e^{i\omega t}\exp((i/\hbar)\hat{H}_0 t)\hat{B}_l^\dagger\exp(-(i/\hbar)\hat{H}_0 t)$ where $\hat{B}_l^\dagger=\sqrt{n_l+1}|(n+1)_l\rangle\langle n_l|$ is the exciton creation operator for chromophore l, and n denotes the excited state (the ground is $|0\rangle$). $\boldsymbol{\mu}_l$ is the transition dipole for chromophore l, and $\boldsymbol{\mu}_l'$ is the permanent dipole in the excited state, while $\boldsymbol{\mu}_l''$ is a quadratic transition dipole which can create double-quantum coherences (overtones); $\boldsymbol{m}_l$, $\boldsymbol{m}_l'$, and $\boldsymbol{m}_l''$ are the corresponding magnetic moments. This model does not take into account permanent dipoles in the ground state and overtones. We can now relate these dipoles to the following transition current: $\boldsymbol{j}_l(\mathbf{k})=-i\omega\boldsymbol{\mu}_l(\mathbf{k})+i\mathbf{k}\times\boldsymbol{m}_l(\mathbf{k})$ where $\boldsymbol{j}_l(\mathbf{k})\equiv\boldsymbol{j}_l\exp(-i\mathbf{k}\mathbf{r}_l)$ (the same is used for other transition currents).

Transforming the first term in Eq. (A2) into the $\mathbf{k}\omega$ domain we obtain

$$\int d\mathbf{r}\hat{\mathbb{J}}(\mathbf{r},t)\cdot\hat{\mathbb{A}}(\mathbf{r},t) = \frac{1}{(2\pi)^5}\int d\omega'\int d\omega''\int d\mathbf{k}\hat{\mathbb{J}}(-\mathbf{k},\omega') \times\hat{\mathbb{A}}(\mathbf{k},\omega'')e^{-i(\omega'+\omega'')t}.$$

This describes an interaction of the system with the optical field of frequency ω'' and wave vector $\mathbf{k}$. Assuming a monochromatic optical field of Eq. (13) and an interaction of field $l=1$ with $+\mathbf{k}_1$ we get

$$\int d\mathbf{r}\hat{\mathbb{J}}(\mathbf{r},t)\cdot\mathbb{A}(\mathbf{r},t)\propto A_0^{(1)}\int d\omega'\mathbf{e}_1\cdot\hat{\mathbb{J}}(-\mathbf{k}_1,\omega')e^{-i(\omega'+\omega_1)t}.$$

Within the RWA $\omega'\approx-\omega_1$. Thus, in the relation $\boldsymbol{j}_l(\mathbf{k})=-i\omega\boldsymbol{\mu}_l(\mathbf{k})+i\mathbf{k}\times\boldsymbol{m}_l(\mathbf{k})$ the optical wave vector and the optical frequency can be used instead of Fourier variables.

For the second term in Eq. (A2) we also assume the RWA so that the interaction frequency is related to the wave vector by $\omega=c|\mathbf{k}|$.

APPENDIX B: ORIENTATIONAL AVERAGINGS TO FIRST-ORDER IN WAVE VECTOR

Orientational averaging $\langle\cdots\rangle$ needs to be performed in order to compute the response functions of the isotropic (randomly oriented) ensembles of molecules.[45] The optical fields, wave vectors, and space coordinates are defined in the laboratory frame, while the transition dipoles and the positions of the chromophores are given in the molecular frame. Molecular susceptibilities need to be averaged over the relative orientation of the two frames. The rotational averaging of n transition currents $\langle\boldsymbol{j}_n^{\nu_n}(\mathbf{k}_n)\cdots\boldsymbol{j}_1^{\nu_1}(\mathbf{k}_1)\rangle \equiv\langle e^{i\mathbf{k}_n\mathbf{r}_n+\cdots+i\mathbf{k}_1\mathbf{r}_1}\boldsymbol{j}_n^{\nu_n}\cdots\boldsymbol{j}_1^{\nu_1}\rangle$ can be calculated to first order in the wave vector when expressing the current through the electric and magnetic transition dipoles. By relating the currents with the transition dipoles and magnetic transition dipoles we have, to the first order in the wave vector, $\boldsymbol{j}_l(\mathbf{k})\approx-i\omega\mu_l-\omega(\mathbf{k}\cdot\mathbf{r}_l)\boldsymbol{\mu}_l+i\mathbf{k}\times\boldsymbol{m}_l$, where the interaction frequency ω is directly related to the wave vector $\omega=c\mathbf{k}$ (for $-\mathbf{k}$ we have to use $-\omega$). A similar expansion can be made for $\boldsymbol{f}$ and $\boldsymbol{g}$.

In isotropic ensemble we should treat each molecule as a collection of transition dipoles with fixed directions in the molecular frame. The laboratory frame coordinates depend on the position of the molecule. We shall replace the coordinates $\mathbf{r}_m$ with $\mathcal{R}+\bar{\mathbf{r}}_m$ where $\mathcal{R}$ is the molecular position in the laboratory frame (the origin of the molecular coordinate system) and $\bar{\mathbf{r}}_m$ is the coordinate of mode m in the molecular frame. We then have $\exp(i\mathbf{k}_n\mathbf{r}_n+\cdots+i\mathbf{k}_1\mathbf{r}_1)=\Phi\exp(i\mathbf{k}_n\bar{\mathbf{r}}_n+\cdots+i\mathbf{k}_1\bar{\mathbf{r}}_1)$ where $\Phi\equiv\exp(i\mathcal{R}(\mathbf{k}_n+\cdots+\mathbf{k}_1))$ is responsible for phase matching and the second factor represents the phase variation of the field within the molecule. The coordinates $\bar{\mathbf{r}}_m$ only vary within each molecule and for molecules smaller than the optical wavelength we have $\mathbf{k}\bar{\mathbf{r}}_m\ll1$, thus an expansion in the wave vector is justified. Performing orientational averagings in the exciton basis, keeping only terms linear in the wave vector, we have $(\mathbf{k}\times\boldsymbol{m})^\nu=\mathbf{k}^{\nu+1}\boldsymbol{m}^{\nu+2}-\mathbf{k}^{\nu+2}\boldsymbol{m}^{\nu+1}$ giving

$$\langle\boldsymbol{j}_{\xi_n}^{\nu_n}(\mathbf{k}_n)\cdots\boldsymbol{j}_{\xi_1}^{\nu_1}(\mathbf{k}_1)\rangle=\Phi(-i)^n\omega_n\cdots\omega_1\Bigg\{\langle\boldsymbol{\mu}_{\xi_n}^{\nu_n}\cdots\boldsymbol{\mu}_{\xi_1}^{\nu_1}\rangle-i\sum_\kappa\mathbf{k}_n^\kappa\langle\bar{\boldsymbol{\mu}}_{\xi_n}^{\kappa,\nu_n}\cdots\boldsymbol{\mu}_{\xi_1}^{\nu_1}\rangle-\cdots-i\sum_\kappa\mathbf{k}_1^\kappa\langle\boldsymbol{\mu}_{\xi_3}^{\nu_3}\cdots\bar{\boldsymbol{\mu}}_{\xi_1}^{\kappa,\nu_1}\rangle - \frac{1}{\omega_n}[\mathbf{k}_n^{\nu_n+1}\langle\boldsymbol{m}_{\xi_n}^{\nu_n+2}\boldsymbol{\mu}_{\xi_{n-1}}^{\nu_{n-1}}\cdots\boldsymbol{\mu}_{\xi_1}^{\nu_1}\rangle-\mathbf{k}_n^{\nu_n+2}\langle\boldsymbol{m}_{\xi_n}^{\nu_n+1}\boldsymbol{\mu}_{\xi_{n-1}}^{\nu_{n-1}}\cdots\boldsymbol{\mu}_{\xi_1}^{\nu_1}\rangle]-\cdots - \frac{1}{\omega_n}[\mathbf{k}_1^{\nu_1+1}\langle\boldsymbol{\mu}_{\xi_n}^{\nu_n}\cdots\boldsymbol{\mu}_{\xi_2}^{\nu_2}\boldsymbol{m}_{\xi_1}^{\nu_1+2}\rangle-\mathbf{k}_1^{\nu_n+2}\langle\boldsymbol{\mu}_{\xi_n}^{\nu_n}\cdots\boldsymbol{\mu}_{\xi_2}^{\nu_2}\boldsymbol{m}_{\xi_1}^{\nu_1+1}\rangle]\Bigg\}, \tag{B1}$$

where $\boldsymbol{\mu}_\xi$ corresponds to an eigenstate transition dipole, and a tensor $\bar{\boldsymbol{\mu}}_\xi^{\kappa,\nu}$ corresponds to $\bar{\boldsymbol{\mu}}_\xi^{\nu',\nu}=\Sigma_n\psi_{\xi n}\bar{\mathbf{r}}_n^{\nu'}\boldsymbol{\mu}_n^\nu$. This expression can be used for any type of transition dipole. The laboratory- frame quantities are now separated from molecular frame vectors and Eqs. (22) and (23) can be used to calculate all the tensor components of the susceptibilities.

Φ needs to be integrated over the active volume where the laser fields overlap. For a finite interaction volume that factor is proportional to $\bar{\Phi}=\sin(\Delta kL)/\Delta k$, where Δk is a wave-vector mismatch, $\Delta k=|\Delta\mathbf{k}|=|\mathbf{k}_n+\cdots+\mathbf{k}_1|$, and L is an interaction size. $\bar{\Phi}$ is a complex function of the sample geometry and laser beam configuration, and it should be taken into consideration in realistic simulations. For $L\to\infty$ the integration of Φ gives $\delta(\mathbf{k}_n+\cdots+\mathbf{k}_1)$ which is the phase-matching condition.

As shown above, the phase-matching direction for the second-order response is given by $\mathbf{n}_1\pm\mathbf{n}_2$. However, the wave vector of the generated signal is $\mathbf{k}_S=\mathbf{n}_S\omega_S/c$ and $|\mathbf{k}_S|=\|\mathbf{k}_1|\pm|\mathbf{k}_2\|$ with $\mathbf{k}_1=\mathbf{n}_1\omega_1/c$ and $\mathbf{k}_2=\mathbf{n}_2\omega_2/c$. These conditions can only be satisfied in a collinear laser configuration. Taking into account the tensor components of isotropic systems such as xyz and $(x)xyy$, all second-order signals vanish in the collinear configuration. The noncollinear geometry where the signal is generated along the phase-matched direction, $\mathbf{n}_1\pm\mathbf{n}_2$, is needed, however, phase matching is not satisfied since the signal wave vector has the phase mismatch $\Delta k=\|\mathbf{k}_1|\pm|\mathbf{k}_2\|-|\mathbf{k}_1\pm\mathbf{k}_2|$.

For the third-order response we have complete phase matching even in collinear configuration, where the signal is finite and yields independent tensor components: $xxyy$, $xyyx$, and $xyxy$ (all three are dipole approximations) and $xxxy$, $xxyx$, and $xyxx$ (these three are first order in $\mathbf{k}$).

APPENDIX C: THE NONLINEAR EXCITON EQUATIONS (NEEs)

The NEEs have been derived previously using the multipolar (μ.E) Hamiltonian and used to calculate the third-order response of excitons.[30,35–38] In this paper we use the minimal-coupling Hamiltonian to extend these equations to include both electric and magnetic interactions and calculate the third- as well as second-order responses.

We start with the Heisenberg equations of motion,

$$i\frac{d}{dt}\langle\hat{F}\rangle=\langle[\hat{F},\hat{H}]\rangle, \tag{C1}$$

where $\hat{F}$ is an operator in the Heisenberg representation $[\hat{F},\hat{H}]=\hat{F}\hat{H}-\hat{H}\hat{F}$, and $\langle\cdots\rangle$ denotes the average over the initial density matrix (where the field is switched off). To calculate the current [Eq. (6)] we need the equations of motion for $\langle\hat{B}\rangle$, $\langle\hat{B}^\dagger\hat{B}\rangle$, $\langle\hat{B}^2\rangle$, and their complex conjugates [Eq. (4)]. These generate higher-order products of $\hat{B}$ and result in an infinite hierarchy of coupled equations. However, from Eq. (4) we see that each interaction with the field can create/annihilate up to two excitons. This means that products of up to four $\hat{B}$ operators can contribute to second-order processes. Without loss of generality we use the Bose commutation relations to bring all the operator products into a normally ordered form where all $\hat{B}^\dagger$ are moved to the left: $\langle\hat{B}^\dagger\cdots\hat{B}^\dagger\hat{B}\cdots\hat{B}\rangle$.[36]

Substituting $\hat{F}\equiv\hat{B}_m$ in Eq. (C1) and taking the expectation value give

$$i\frac{d}{dt}B_m=\sum_n h_{mn}B_n+\sum_{nkl}V_{mnkl}Z_{nkl}-\tilde{j}_m^*-\tilde{f}_mB_m-2\tilde{g}_m^*B_m^*, \tag{C2}$$

where $B_m\equiv\langle\hat{B}_m\rangle$, $Z_{nkl}\equiv\langle\hat{B}_n^\dagger\hat{B}_k\hat{B}_l\rangle$, $h_{mm}=\varepsilon_m$, $\tilde{j}_m(t)\equiv\tilde{j}_m^{(1)}(t)+\tilde{j}_m^{(2)}(t)$, $\tilde{f}_m(t)\equiv\tilde{f}_m^{(1)}(t)+\tilde{f}_m^{(2)}(t)$, $\tilde{g}_m(t)\equiv\tilde{g}_m^{(1)}(t)+\tilde{g}_m^{(2)}(t)$, and the anharmonicity parameter $V_{mnkl}\equiv U_{mnkl}+U_{nmkl}$. Here we use $\tilde{j}_m^{(1)}(t)\equiv(1/c)\boldsymbol{j}_m\cdot\mathbb{A}(\mathbf{r}_m,t)$ and $\tilde{j}_m^{(2)}(t)=(1/c)\boldsymbol{j}'_m\mathbb{A}^2(\mathbf{r}_m,t)$; the same notation is used for $\tilde{f}_m$ and $\tilde{g}_m$. The interaction with each parameter $\tilde{j}_m$, $\tilde{f}_m$, and $\tilde{g}_m$ with an nth-order variable creates a higher-order variable of order $n+1$ [for $\tilde{j}_m^{(1)}\cdots$] or order $n+2$ [for $\tilde{j}_m^{(2)}\cdots$].

In the second-order response we consider processes involving different incoming and outgoing frequencies and take into account $\tilde{f}_m$ and $\tilde{g}_m$. For the third-order responses we invoke the RWA and neglect $\tilde{f}_m$ and $\tilde{g}_m$.

B are coupled to the Z variables. Using Eq. (C1) we get

$$\begin{aligned}i\frac{d}{dt}Z_{lmn}=&\sum_j[-h_{jl}Z_{lmn}+h_{jm}Z_{lnj}+h_{jn}Z_{lmj}]\\&+\sum_{kj}V_{mn,kj}Z_{lkj}+\tilde{j}_lY_{mn}-\tilde{j}_m^*N_{ln}-\tilde{j}_n^*N_{lm}\\&-2\delta_{mn}\tilde{g}_m^*B_l^*.\end{aligned} \tag{C3}$$

Here $Y_{mn}\equiv\langle\hat{B}_m\hat{B}_n\rangle$, and $N_{mn}\equiv\langle\hat{B}_m^\dagger\hat{B}_n\rangle$. In Eq. (C3) and hereafter we neglect products of more than four $\hat{B}$ operators that do not contribute to the second- and third-order responses. The new variables Y satisfy

$$\begin{aligned}i\frac{d}{dt}Y_{mn}=&\sum_j[h_{jm}Y_{nj}+h_{jn}Y_{mj}]+\sum_{kl}V_{mn,kl}Y_{kl}-\tilde{j}_m^*B_n\\&-\tilde{j}_n^*B_m-(\tilde{f}_m+\tilde{f}_n)Y_{mn}-2\delta_{mn}\tilde{g}_m^*.\end{aligned} \tag{C4}$$

The variables $N_{mn}\equiv\langle\hat{B}_m^\dagger\hat{B}_n\rangle$ satisfy

$$\begin{aligned}i\frac{d}{dt}N_{mn}=&\sum_j[-h_{jm}N_{mn}+h_{jn}N_{mj}]+\sum_{jkl}V_{njkl}X_{mjkl}\\&-\sum_{jkl}W_{jklm}X_{jknl}-\tilde{j}_n^*B_m^*+\tilde{j}_mB_n\\&-2\tilde{g}_n^*Y_{mn}^*+2\tilde{g}_mY_{mn},\end{aligned} \tag{C5}$$

where $W_{mnkl}\equiv U_{mnkl}+U_{mnlk}$, and $X_{mnkl}\equiv\langle\hat{B}_m^\dagger\hat{B}_n^\dagger\hat{B}_k\hat{B}_l\rangle$ are new variables which satisfy the following equation

$$\begin{aligned}i\frac{d}{dt}X_{mnkl}=&-\sum_j[h_{jm}X_{jnkl}+h_{jn}X_{mjkl}]\\&+\sum_j[h_{jk}X_{mnjl}+h_{jl}X_{mnkj}]\\&+\sum_{jj'}[V_{kljj'}X_{mnjj'}-W_{jj'mn}X_{jj'kl}]\\&-2\delta_{kl}\tilde{g}_k^*Y_{mn}^*+2\delta_{mn}\tilde{g}_mY_{kl}.\end{aligned} \tag{C6}$$

This closes the hierarchy of equations for our model defined by Eqs. (1)–(5). The second-order responses are obtained in

Appendix E by expanding these equations order by order in the optical field. Rather than deriving general expressions we shall focus on specific techniques. By retaining the dominant resonant terms in the RWA we find that fewer equations are needed in each case which considerably simplify the results.

APPENDIX D: THE LINEAR RESPONSE

The linear-response function is calculated by solving Eq. (C2) to first order in the field. The first-order variable $B^{(1)}$ describes the single-exciton evolution,

$$i\frac{d}{d\tau}B_m^{(1)} = \sum_n h_{mn}B_n^{(1)} - \tilde{j}_m^{(1)*}(\tau). \tag{D1}$$

The solution of Eq. (D1) is given by the one-exciton Green's function $G(\tau)$,

$$B_m^{(1)}(\tau) = i\int d\tau' \sum_n G_{mn}(\tau-\tau')\tilde{j}_n^{(1)*}(\tau'), \tag{D2}$$

which satisfies the following equation:

$$\frac{dG_{m,n}(\tau)}{d\tau} + i\sum_{n'} h_{m,n'}G_{n',n}(\tau) = \delta(\tau). \tag{D3}$$

This equation can be solved using the one-exciton eigenenergies Ω_ξ and eigenvectors $\psi_{\xi m}$ [Eq. (2)]. We then have

$$G_{m,n}(\tau) = \sum_\xi \psi_{\xi m}I_\xi(\tau)\psi_{\xi n}^*, \tag{D4}$$

where

$$I_\xi(\tau) = \theta(\tau)\exp(-i\Omega_\xi\tau - \gamma_\xi\tau), \tag{D5}$$

γ_ξ is a dephasing rate of the ξ exciton, and $\theta(\tau)$ is the Heaviside step function [$\theta(\tau)=0$ for $\tau<0$ and $\theta(\tau)=1$ for $\tau\geqslant 0$] which guarantees causality.

The following linear induced current is obtained from Eq. (4):

$$\mathbb{J}^{(1)}(\mathbf{r},\tau) = \sum_m \langle \boldsymbol{j}_m(\mathbf{r})B_m^{(1)}(\tau)\rangle + \text{c.c.}, \tag{D6}$$

where $\boldsymbol{j}_m^\nu(\mathbf{r}) \equiv \delta(\mathbf{r}-\mathbf{r}_m)\boldsymbol{j}_m^\nu$ and $\langle\ \rangle$ now stands for orientational averaging. Combining Eqs. (D2), (D6), and (7) we obtain the following linear-response function:

$$R_{\nu_2\nu_1}^{(1)}(\mathbf{r}_2,\tau_2,\mathbf{r}_1,\tau_1) = \frac{i}{c}\sum_{n_2n_1}\langle \boldsymbol{j}_{n_2}^{\nu_2}(\mathbf{r}_2)\boldsymbol{j}_{n_1}^{*\nu_1}(\mathbf{r}_1)\rangle G_{n_2n_1}(\tau_2-\tau_1) + \text{c.c.}, \tag{D7}$$

which in the eigenstate basis is

$$R_{\nu_2\nu_1}^{(1)}(-\mathbf{k}_2,\tau_2,\mathbf{k}_1,\tau_1) = \frac{i}{c}\sum_\xi \langle \boldsymbol{j}_{\xi_2}^{\nu_2}(-\mathbf{k}_2)\boldsymbol{j}_{\xi_1}^{*\nu_1}(-\mathbf{k}_1)\rangle I_\xi(\tau_2-\tau_1) + \text{c.c.} \tag{D8}$$

The time Fourier transformation of this function gives the linear susceptibility [Eq. (25)].

APPENDIX E: NEE FOR THE SECOND-ORDER RESPONSE

In this appendix we give general NEE up to second order including the Q interaction operator.

Equations (C2)–(C6) are expanded order by order in the fields. To the first order we get

$$i\frac{d}{dt}B_m^{(1)} = \sum_n h_{mn}B_n^{(1)} - \tilde{j}_m^{(1)*}, \tag{E1}$$

$$i\frac{d}{dt}Y_{mn}^{(1)} = \sum_j [h_{jm}Y_{nj}^{(1)} + h_{jn}Y_{mj}^{(1)}] + \sum_{kl} V_{mn,kl}Y_{kl}^{(1)} - 2\delta_{mn}\tilde{g}_m^{(1)*}. \tag{E2}$$

The second-order equations are

$$i\frac{d}{dt}B_m^{(2)} = \sum_n h_{mn}B_n^{(2)} + \sum_{nkl} V_{mnkl}Z_{nkl}^{(2)} - j_m^{(2)*} - \tilde{f}_m^{(1)}B_m^{(1)} - 2\tilde{g}_m^{(1)*}B_m^{(1)*}, \tag{E3}$$

$$i\frac{d}{dt}Y_{mn}^{(2)} = \sum_j [h_{jm}Y_{nj}^{(2)} + h_{jn}Y_{mj}^{(2)}] + \sum_{kl} V_{mn,kl}Y_{kl}^{(2)} - \tilde{j}_m^{(1)*}B_n^{(1)} - \tilde{j}_n^{(1)*}B_m^{(1)} - (\tilde{f}_m^{(1)} + \tilde{f}_n^{(1)})Y_{mn}^{(1)} - 2\delta_{mn}\tilde{g}_m^{(2)*}, \tag{E4}$$

$$i\frac{d}{dt}N_{mn}^{(2)} = \sum_j [-h_{jm}N_{mn}^{(2)} + h_{jn}N_{mj}^{(2)}] + \sum_{jkl} V_{njkl}X_{mjkl}^{(2)} - \sum_{jkl} W_{jklm}X_{jknl}^{(2)} - \tilde{j}_n^{(1)*}B_m^{(1)*} + \tilde{j}_m^{(1)}B_n^{(1)} - 2\tilde{g}_n^{(1)*}Y_{mn}^{(1)*} + 2\tilde{g}_m^{(1)}Y_{mn}^{(1)}, \tag{E5}$$

$$i\frac{d}{dt}Z_{lmn}^{(2)} = \sum_j [-h_{jl}Z_{lmn}^{(2)} + h_{jm}Z_{lnj}^{(2)} + h_{jn}Z_{lmj}^{(2)}] + \sum_{kj} V_{mn,kj}Z_{lkj}^{(2)} + \tilde{j}_l^{(1)}Y_{mn}^{(1)} - 2\delta_{mn}\tilde{g}_m^{(1)*}B_m^{(1)*}, \tag{E6}$$

$$i\frac{d}{dt}X_{mnkl}^{(2)} = -\sum_j [h_{jm}X_{jnkl}^{(2)} + h_{jn}X_{mjkl}^{(2)}] + \sum_j [h_{jk}X_{mnjl}^{(2)} + h_{jl}X_{mnkj}^{(2)}] + \sum_{jj'} [V_{kljj'}X_{mnjj'}^{(2)} - W_{jj'mn}X_{jj'kl}^{(2)}] - 2\delta_{kl}\tilde{g}_k^{(1)*}Y_{mn}^{(1)*} + 2\delta_{mn}\tilde{g}_m^{(1)}Y_{kl}^{(1)}. \tag{E7}$$

The closed Green's-function expressions for the solution of these equations can be derived. These equations are simplified considerably in the absence of pure dephasing whereby $Z=B^*Y$ and $N=B^*B$ and only Eqs. (E1)–(E4) are required for all the second-order signals.

An improved approximation is obtained by assuming factorized forms for the relaxation operator of Z and X variables as shown in Ref. 36. Then the Green's function of Z (rather than Z itself) is factorized into a product of the Green's functions of the B and Y variables. In that case the

exciton scattering matrix can be used to get population relaxation (the latter is completely neglected if we factorize Z). For resonant second-order techniques this can be used to describe DFG more complete than in Appendix F.

Nonresonant techniques must include all the variables B, Y, N, Z, and X, which make the description very complicated. In this case pure state factorization may be necessary to perform calculations for large systems since the number of equations for Z and X grows up very rapidly with system size.

APPENDIX F: FREQUENCY-DOMAIN SECOND-ORDER SIGNALS

1. Derivation of the SFG susceptibility

The SFG signal is calculated by solving Eqs. (C2)–(C6) order by order. There is only one first-order variable $B^{(1)}$, which describes the single-exciton evolution, which is given by Eq. (D1). For the second-order variables [Eq. (C4)] we find

$$i\frac{d}{d\tau}Y^{(2)}_{mn}=\sum_j [h_{jm}Y^{(2)}_{nj}+h_{jn}Y^{(2)}_{mj}]+\sum_{kl} V_{mn,kl}Y^{(2)}_{kl} - \tilde{j}^{(1)*}_m(\tau)B^{(1)}_n-\tilde{j}^{(1)*}_n(\tau)B^{(1)}_m, \tag{F1}$$

which requires the calculation of two-exciton resonances.

The two-exciton evolution is described by the two-exciton Green's function $\mathcal{G}^Y$,

$$Y^{(2)}_{mn}(\tau)=i\int d\tau' \sum_{m'n'} \mathcal{G}^Y_{mnm'n'}(\tau-\tau')[2\tilde{j}^{(1)*}_{m'}(\tau')B^{(1)}_{n'}(\tau')], \tag{F2}$$

which satisfies the following equation:

$$\frac{d\mathcal{G}^Y_{mn,m'n'}}{dt}+i\sum_{m''n''}(h^{(Y)}_{mn,m''n''}+V_{mn,m''n''})\mathcal{G}^Y_{m''n'',m'n'}=\delta(\tau). \tag{F3}$$

To solve this equation we first calculate the zero-order noninteracting ($V=0$) two-exciton Green's function $\mathcal{G}$, which may be factorized into a product of one-exciton Green's functions $\mathcal{G}_{mn,m'n'}(\tau)=G_{m,m'}(\tau)G_{n,n'}(\tau)$. $\mathcal{G}^Y$ is connected to $\mathcal{G}$ by the Bethe-Salpeter equation,[35]

$$\mathcal{G}^Y(\tau)=\mathcal{G}(\tau)+\int_0^\tau d\tau' \int_0^{\tau'} d\tau_1 \mathcal{G}(\tau-\tau')\Gamma(\tau'-\tau_1)\mathcal{G}(\tau_1), \tag{F4}$$

where Γ is the *two-exciton scattering matrix*. Both $\mathcal{G}^Y$ and Γ are tetradic matrices. The scattering matrix is causal and vanishes for $\tau'<\tau_1$.

A compact expression for $\Gamma(t)$ is obtained by transforming it to the frequency domain,[35,37]

$$\Gamma(\omega)=-iV(1+i\mathcal{G}(\omega)V)^{-1}, \tag{F5}$$

with the noninteracting two-exciton Green's function,

$$\mathcal{G}_{mn,m'n'}(\omega)=\sum_{\xi\xi'}\psi_{\xi m}\psi_{\xi' n}\mathcal{I}_{\xi\xi'}(\omega)\psi^*_{\xi m'}\psi^*_{\xi' n'}, \tag{F6}$$

and

$$\mathcal{I}_{\xi\xi'}(\omega)=\frac{i}{\omega-\Omega_\xi-\Omega_{\xi'}+i(\gamma_\xi+\gamma_{\xi'})}. \tag{F7}$$

The calculation of the scattering matrix requires the inversion of the matrix $D=1+i\mathcal{G}(\omega)V$. Using Eq. (F5) we find $-iV\mathcal{G}^Y=\Gamma(\omega)\mathcal{G}(\omega)$ and

$$\Gamma(\omega)=-iVD^{-1}(\omega). \tag{F8}$$

We will use both matrices Γ and D^{-1} in our final expressions. Γ is the two-exciton scattering matrix. The required numerical effort is considerably reduced for localized excitons with short-range anharmonicities and for periodic systems.[35,37]

The following SFG polarization is finally obtained from Eq. (4):

$$J^{\mathrm{SFG}}(\mathbf{r},\tau)=\sum_m \langle \boldsymbol{g}_m(\mathbf{r})Y^{(2)}_{mm}(\tau)\rangle+\mathrm{c.c.}, \tag{F9}$$

where $\boldsymbol{g}_n(\mathbf{r})\equiv\delta(\mathbf{r}-\mathbf{r}_n)\boldsymbol{g}_n$ (and similarly for $\boldsymbol{\mu}$ and $\boldsymbol{p}$) and $\langle\ \rangle$ now stands for rotational averaging. Combining Eqs. (D2), (F2), and (F9) and relation (7) we obtain the following SFG response function:

$$R^{\mathrm{SFG}}_{\nu_3\nu_2\nu_1}(\mathbf{r}_3,\tau_3,\mathbf{r}_2,\tau_2,\mathbf{r}_1,\tau_1) =2\frac{i^2}{c^2}\sum_{\mathrm{perm}_2}\sum_{n_3n_2n_1}\langle \boldsymbol{g}^{\nu_3}_{n_3}(\mathbf{r}_3)\boldsymbol{j}^{*\nu_2}_{n_2}(\mathbf{r}_2)\boldsymbol{j}^{*\nu_1}_{n_1}(\mathbf{r}_1)\rangle \times\sum_m \mathcal{G}^Y_{n_3n_3mn_2}(\tau_3-\tau_2)G_{mn_1}(\tau_2-\tau_1)+\mathrm{c.c.} \tag{F10}$$

Here Σ_{perm2} denotes the sum over the two permutations of the indices $\nu_1\mathbf{r}_1\tau_1$ and $\nu_2\mathbf{r}_2\tau_2$.

The response functions can be expressed in terms of one-exciton Green's functions using Eq. (F4). The following susceptibility is obtained from Eqs. (9) and (F10):

$$X^{\mathrm{SFG}}_{\nu_3\nu_2\nu_1}(-\mathbf{k}_3,-\omega_3,\mathbf{k}_2,\omega_2,\mathbf{k}_1,\omega_1) =2\pi\frac{i^2}{c^2}\delta(\omega_3-\omega_2-\omega_1) \times\sum_{\mathrm{perm}_2}\sum_{n_3n_2n_1}2\langle \boldsymbol{g}^{\nu_3}_{n_3}(-\mathbf{k}_3)\boldsymbol{j}^{*\nu_2}_{n_2}(-\mathbf{k}_2)\boldsymbol{j}^{*\nu_1}_{n_1}(-\mathbf{k}_1)\rangle \times\sum_{mn_3'n_2'}D^{-1}_{n_3n_3,n_3'n_2'}(\omega_2+\omega_1) \times\mathcal{G}_{n_3'n_2',mn_2}(\omega_2+\omega_1)G_{mn_1}(\omega_1)+\mathrm{c.c.}'. \tag{F11}$$

Here $\boldsymbol{g}_n(\mathbf{k})\equiv\exp(i\mathbf{k}\mathbf{r}_n)\boldsymbol{g}_n$, $\boldsymbol{j}_n(\mathbf{k})\equiv\exp(i\mathbf{k}\mathbf{r}_n)\boldsymbol{j}_n$, and Σ_{perm_2} is over the two permutations of $\nu_1\mathbf{k}_1\omega_1$ and $\nu_2\mathbf{k}_2\omega_2$.

Numerical simulations can be best carried out in the exciton basis. Using Eqs. (D4) and (F6) and defining

$$D^{-1}_{\xi_4\xi_3\xi_2\xi_1}\equiv\sum_{n_4n_3n_2n_1}\psi^*_{\xi_4n_4}\psi^*_{\xi_4n_4}\psi_{\xi_4n_4}\psi_{\xi_4n_4}D^{-1}_{n_4n_3n_2n_1}, \tag{F12}$$

we transform Eq. (F11) and obtain Eq. (26).

2. Derivation of the DFG susceptibility

We next calculate the susceptibility of the DFG signal defined in Sec. V B 1 by solving Eqs. (C2)–(C6) within the RWA. The first-order variable B is given by Eq. (D1). The second-order variable [Eq. (C5)] is

$$i\frac{d}{dt}N^{(2)}_{mn}=\sum_j\left[-h_{jm}N^{(2)}_{mn}+h_{jn}N^{(2)}_{mj}\right]-\tilde{j}^{(1)*}_n B^{(1)*}_m+\tilde{j}^{(1)}_m B^{(1)}_n. \tag{F13}$$

Equations (D1) and (F13) describe the polarization [see Eq. (4)],

$$J^{\mathrm{DFG}}(\mathbf{r},t)=\sum_m \boldsymbol{f}_m(\mathbf{r})N^{(2)}_{mm}(t). \tag{F14}$$

Note that this signal does not depend on the anharmonicity and the anharmonic variables X [X is generated by $Y^{(1)}$ as is seen from Eq. (C6)]. $B^{(1)}$ is given by Eq. (D2). In the absence of pure dephasing we can factorize $N^{(2)}=B^{(1)*}B^{(1)}$. Equations (7), (D2), and (F14) then give

$$\begin{aligned}R^{\mathrm{DFG}}_{\nu_3\nu_2\nu_1}&(\mathbf{r}_3,\tau_3,\mathbf{r}_2,\tau_2,\mathbf{r}_1,\tau_1)\\&=-\frac{i^2}{c^2}\sum_{\mathrm{perm}_2}\sum_{n_3n_2n_1}\langle \boldsymbol{f}^{\nu_3}_{n_3}(\mathbf{r}_3)\boldsymbol{j}^{\nu_2}_{n_2}(\mathbf{r}_2)\boldsymbol{j}^{*\nu_1}_{n_1}(\mathbf{r}_1)\rangle\\&\quad\times G^{\dagger}_{n_3n_2}(\tau_3-\tau_2)G_{n_3n_1}(\tau_3-\tau_1),\end{aligned} \tag{F15}$$

and the following DFG susceptibility is finally obtained from Eq. (9):

$$\begin{aligned}X^{\mathrm{DFG}}_{\nu_3\nu_2\nu_1}&(-\mathbf{k}_3,-\omega_3,\mathbf{k}_2,\omega_2,\mathbf{k}_1,\omega_1)\\&=-2\pi\frac{i^2}{c^2}\delta(\omega_3-\omega_2-\omega_1)\\&\quad\times\sum_{\mathrm{perm}_2}\sum_{n_3n_2n_1}\langle \boldsymbol{f}^{\nu_3}_{n_3}(-\mathbf{k}_3)\boldsymbol{j}^{\nu_2}_{n_2}(-\mathbf{k}_2)\boldsymbol{j}^{*\nu_1}_{n_1}(-\mathbf{k}_1)\rangle\\&\quad\times G^{*}_{n_3n_2}(-\omega_2)G_{n_3n_1}(\omega_1).\end{aligned} \tag{F16}$$

[1] In *Circular Dichroism: Principles and Applications*, 2nd ed., edited by N. Berova, K. Nakanishi, and R. W. Woody (Wiley, New York, 2000).
[2] L. A. Nafie, Annu. Rev. Phys. Chem. **48**, 357 (1997).
[3] L. D. Barron, *Molecular Light Scattering and Optical Activity*, 2nd ed. (Cambridge University Press, Cambridge, 2004).
[4] L. D. Barron, E. W. Blanch, I. H. McColl, C. D. Syme, L. Hecht, and K. Nielsen, Spectroscopy-An International Journal, IDS Number: 665MB, ISSN: 0712-4813, **17**, 101 (2003).
[5] I. H. McColl, E. W. Blanch, A. C. Gill, A. G. O. Rhie, L. Ritchie, M. A. Hecht, K. Nielsen, and L. D. Barron, J. Am. Chem. Soc. **125**, 10019 (2003).
[6] F. Eker, X. Cao, L. A. Nafie, Q. Huang, and R. Schweitzer-Stenner, J. Phys. Chem. B **107**, 358 (2003).
[7] T. Wagersreiter and S. Mukamel, J. Chem. Phys. **105**, 7995 (1996).
[8] N. J. Greenfield, Anal. Biochem. **235**, 1 (1996).
[9] N. Sreerama and R. W. A. Woody, Anal. Biochem. **287**, 252 (2000).
[10] N. Sreerama and R. W. Woody, Protein Sci. **12**, 384 (2003).
[11] D. H. Chin, R. W. Woody, C. A. Rohl, and R. L. Baldwin, Proc. Natl. Acad. Sci. U.S.A. **99**, 15416 (2002).
[12] N. Sreerama, S. Y. Venyaminov, and R. W. Woody, Protein Sci. **8**, 370 (1999).
[13] N. Sreerama, R. W. Venyaminov, and S. Y. Woody, Anal. Biochem. **287**, 243 (2000).
[14] M. T. Zanni, N.-H. Ge, Y. S. Kim, and R. M. Hochstrasser, Proc. Natl. Acad. Sci. U.S.A. **98**, 11265 (2001).
[15] A. Piryatinski, V. Chernyak, and S. Mukamel, Chem. Phys. **266**, 285 (2001).
[16] A. Piryatinski, S. A. Asher, and S. Mukamel, J. Phys. Chem. **106**, 3524 (2002).
[17] E. C. Fulmer, P. Mukherjee, A. T. Krummel, and M. T. Zanni, J. Chem. Phys. **120**, 8067 (2004).
[18] A. D. Buckingham and P. Fischer, in *Chirality: Physical Chemistry*, edited by J. M. Hicks (Oxford University Press, New York, 2002), pp. 119–129.
[19] B. Champagne, P. Fischer, and A. D. Buckingham, Chem. Phys. Lett. **331**, 83 (2000).
[20] M. A. Belkin, T. A. Kulakov, K. H. Ernst, L. Yan, and Y. R. Shen, Phys. Rev. Lett. **85**, 4474 (2000).
[21] N. I. Koroteev, V. A. Makarov, and S. N. Volkov, Opt. Commun. **157**, 111 (1998).
[22] M. Cho, J. Chem. Phys. **116**, 1562 (2002).
[23] S. Cheon and M. Cho, Phys. Rev. A **71**, 013808 (2005).
[24] K. Wynne, J. Chem. Phys. **122**, 244503 (2005).
[25] T. Kobayashi, *J-Aggregates* (World Scientific, Singapore, 1996).
[26] H. van Amerogen, L. Valkunas, and R. van Grondelle, *Photosynthetic Excitons* (World Scientific, Singapore, 2000).
[27] M. Pope and C. E. Swenberg, *Electron Processes in Organic Crystals* (Oxford University Press, New York, 1999).
[28] P. Hamm, M. Lim, and R. M. Hochstrasser, J. Phys. Chem. B **102**, 6123 (1998).
[29] S. Mukamel, Annu. Rev. Phys. Chem. **51**, 691 (2000).
[30] A. Piryatinski, V. Chernyak, and S. Mukamel, Chem. Phys. **266**, 311 (2001).
[31] A. M. Moran, S.-M. Park, J. Dreyer, and S. Mukamel, J. Chem. Phys. **118**, 3651 (2003).
[32] C. Fang, J. Wang, Y. S. Kim, A. K. Charnley, W. Barber-Armstrong, A. B. Smith III, S. M. Decatur, and R. M. Hochstrasser, J. Phys. Chem. B **108**, 10415 (2004).
[33] R. W. Woody, Monatsch. Chem. **136**, 347 (2005).
[34] A. Davydov, *A Theory of Molecular Excitons* (McGraw-Hill, New York, 1962).
[35] J. A. Leegwater and S. Mukamel, Phys. Rev. A **46**, 452 (1992).
[36] V. Chernyak, W. M. Zhang, and S. Mukamel, J. Chem. Phys. **109**, 9587 (1998).
[37] D. Abramavicius and S. Mukamel, J. Chem. Phys. **122**, 134305 (2005).
[38] D. Abramavicius and S. Mukamel, Chem. Phys. **318**, 50 (2005).
[39] W. M. Zhang, V. Chernyak, and S. Mukamel, J. Chem. Phys. **110**, 5011 (1999).
[40] D. P. Craig and T. Thirunamachandran, *Molecular Quantum Electrodynamics* (Dover, New York, 1998).
[41] C. Cohen-Tannoudji, J. Dupont-Roc, and G. Grynberg, *Atom-Photon Interactions* (Wiley, New York, 1992).
[42] S. Mukamel, *Principles of Nonlinear Optical Spectrscopy* (Oxford University Press, New York, 1995).
[43] Note that in our previous papers (Refs. 37 and 38) we used a different definition of the Fourier transform with an opposite sign of the wave vector.
[44] S. Tanaka, V. Chernyak, and S. Mukamel, Phys. Rev. A **63**, 063405 (2001).
[45] D. L. Andrews and T. Thirunamachandran, J. Chem. Phys. **67**, 5026 (1977).
[46] Y. R. Shen, *The Principles of Nonlinear Optics* (Wiley, New York, 1984).
[47] F. C. Spano and S. Mukamel, Phys. Rev. A **40**, 5783 (1989).
[48] F. C. Spano and S. Mukamel, Phys. Rev. Lett. **66**, 1197 (1991).
[49] R. W. Woody, J. Chem. Phys. **49**, 4797 (1968).
[50] P. M. Bayley, E. B. Nielsen, and J. A. Shellman, J. Phys. Chem. **73**, 228 (1969).
[51] D. L. Andrews, J. Phys. B **13**, 4091 (1980).
[52] P. A. D. L. Andrews, *Optical Harmonics in Molecular Systems* (Wiley-VCH, NY, 2002).
[53] I. Freund and P. M. Rentzepis, Phys. Rev. Lett. **18**, 393 (1967).
[54] M. A. Belkin, S. H. Han, X. Wei, and Y. R. Shen, Phys. Rev. Lett. **87**, 113001 (2001).
[55] P. Fischer, A. D. Buckingham, and A. C. Albrecht, Phys. Rev. A **64**, 053816 (2001).
[56] A. Bonvalet, J. Nagle, V. Berger, A. Migus, J. L. Martin, and M. Joffre, Phys. Rev. Lett. **76**, 4392 (1996).
[57] B. Dick, G. Stegeman, R. Twieg, and J. Zyss, Chem. Phys. Molecular Nonlinear Optics: Materials, Phenomena and Devices (Special Issue)

245 (1999).
[58] N. Belabas and M. Joffre, Opt. Lett. **27**, 2043 (2002).
[59] G. J. Simpson, J. Chem. Phys. **117**, 3398 (2002).
[60] S. Roke, A. Kleyn, and M. Bonn, Chem. Phys. Lett. **370**, 227 (2003).
[61] A. J. Moad and G. J. Simpson, J. Phys. Chem. B **108**, 3548 (2004).
[62] M. Bonn, H. Ueba, and M. Wolf, J. Phys.: Condens. Matter **17**, S201 (2005).
[63] R. Venkatramani and S. Mukamel, J. Phys. Chem. B **109**, 8132 (2005).
[64] V. A. Apkarian, C. J. Bardeen, J. Che, P. Cong, B. Kohler, J. L. Krause, C. C. Martens, M. Messina, K. R. Wilson, V. V. Yakovlev *et al.*, *Ultrafast Phenomena X* (Springer-Verlag, Berlin, 1996), p. 219.
[65] N. Demirdöven, C. M. Cheatum, H. S. Chung, M. Khalil, J. Knoester, and A. Tokmakoff, J. Am. Chem. Soc. **126**, 7981 (2004).
[66] M. L. Cowan, B. D. Bruner, N. Huse, J. R. Dwyer, B. Chugh, E. T. J. Nibbering, T. Elsaesser, and R. J. D. Miller, Nature (London) **434**, 199 (2005).
[67] Z. Chi, X. G. Chen, S. W. Holtz, and S. A. Asher, Biochemistry **37**, 2854 (1998).
[68] D. Abramavicius, W. Zhuang, and S. Mukamel, J. Phys. Chem. B **108**, 18034 (2004).
[69] D. Zeidler, S. Frey, K.-L. Kompa, and M. Motzkus, Phys. Rev. A **64**, 023420 (2001).
[70] G. D. Scholes, J. Chem. Phys. **121**, 10104 (2004).
[71] T. Brixner, G. Krampert, T. Pfeifer, R. Selle, G. Gerber, M. Wollenhaupt, O. Graefe, C. Horn, D. Liese, and T. Baumert, Phys. Rev. Lett. **92**, 208301 (2004).
[72] B. Brüggemann and V. May, Chem. Phys. Lett. **400**, 573 (2004).
[73] B. Brüggemann and V. May, J. Phys. Chem. B **108**, 10529 (2004).